Solar Energetic Particle Events in the 23rd Solar Cycle: Interplanetary Magnetic Field Configuration and Statistical Relationship with Flares and CMEs

R. Miteva · K.-L. Klein · O. Malandraki · G. Dorrian

Abstract We study the influence of the large-scale interplanetary magnetic field configuration on the solar energetic particles (SEPs) as detected at different satellites near Earth and on the correlation of their peak intensities with the parent solar activity. We selected SEP events associated with X- and M-class flares at western longitudes, in order to ensure good magnetic connection to Earth. These events were classified into two categories according to the global interplanetary magnetic field (IMF) configuration present during the SEP propagation to 1 AU: standard solar wind or interplanetary coronal mass ejections (ICMEs). Our analysis shows that around 20 % of all particle events are detected when the spacecraft is immersed in an ICME. The correlation of the peak particle intensity with the projected speed of the SEP-associated coronal mass ejection is similar in the two IMF categories of proton and electron events, ≈ 0.6. The SEP events within ICMEs show stronger correlation between the peak proton intensity and the soft X-ray flux of the associated solar flare, with correlation coefficient $r = 0.67 \pm 0.13$, compared to the SEP events propagating in the standard solar wind, $r = 0.36 \pm 0.13$. The difference is more pronounced for near-relativistic electrons. The main reason for the different correlation behavior seems to be the larger spread of the flare longitude in the SEP sample detected in the solar wind as compared to SEP events within ICMEs. We discuss to what

R. Miteva (✉) · K.-L. Klein
LESIA-Observatoire de Paris, CNRS, UPMC Univ. Paris 06, Univ. Paris-Diderot, 5 place Jules Janssen, 92195 Meudon, France
e-mail: rositsa.miteva@obspm.fr

K.-L. Klein
e-mail: ludwig.klein@obspm.fr

O. Malandraki · G. Dorrian
Institute of Astronomy, Astrophysics, Space Applications and Remote Sensing, National Observatory of Athens, Athens, Greece

O. Malandraki
e-mail: omaland@astro.noa.gr

G. Dorrian
e-mail: gdorrian@astro.noa.gr

extent observational bias, different physical processes (particle injection, transport, *etc.*), and the IMF configuration can influence the relationship between SEPs and coronal activity.

1. Introduction

Solar energetic particles (SEPs) are transient enhancements of the intensities of energetic protons, ions, and electrons observed in the interplanetary (IP) space. They are known to follow in time eruptive phenomena in the solar corona, such as flares and coronal mass ejections (CMEs). Both small scale processes during flares and CME-driven shock waves are used to explain the particle acceleration (see, *e.g.*, the review of Klecker *et al.*, 2006). The question how flares and CMEs affect SEPs is, however, largely unresolved, because particle measurements near 1 AU are related to the coronal accelerator through a poorly understood chain of processes of acceleration, access to, and propagation in the dynamic interplanetary medium.

One approach to identify physical relationships between SEPs and the parent solar activity is statistical. Numerous studies have shown that SEP events are associated both with flares, as manifested, *e.g.*, by their soft X-ray (Garcia, 2004) or radio (Kahler, 1982a, 1982b) emission, and with fast and broad coronal mass ejections (Kahler, 1992; Reames, 1999). The recent global study of SEP events in the 23rd solar cycle by Cane, Richardson, and von Rosenvinge (2010) confirmed this. Pure cases of SEP events in association with fast CMEs lacking evidence of other, flare-like, acceleration processes in the corona are rare (Kahler *et al.*, 1986) or non-existent (Marqué, Posner, and Klein, 2006). On the other hand, strong flares that are not accompanied by CMEs are not associated with SEP events (detectable by GOES) either, mostly because the flare-accelerated particles remain confined in coronal magnetic fields (Klein, Trottet, and Klassen, 2010; Klein *et al.*, 2011).

More detailed statistical studies tried to relate the peak intensity of SEP events to parameters of the flare or the CME. Chertok (1990) showed a close correlation between peak proton intensities measured in space and gamma-ray line fluxes, but others concluded that the ratio between the numbers of deka-MeV protons emitting gamma-ray lines and detected *in situ* varied considerably from event to event (Cliver *et al.*, 1989; Ramaty *et al.*, 1993). There are also indications for some statistical correlations between SEP intensities and microwave burst parameters (Kahler, 1982b). Garcia (2004) developed a very detailed empirical analysis relating the proton intensity at energies above 10 MeV to a combination of parameters of the soft X-ray (SXR) burst (peak flux, duration, and emission measure). Correlations between SEP peak intensities and CME parameters were also found, especially with the plane-of-the-sky speed of CMEs (Kahler, 2001). The reported correlation coefficients range between 0.6 and 0.7. Since the significance of correlation coefficients was either not assessed, or only confidence levels were given, it is hard to see if any difference in the correlation coefficients is statistically significant. The large scatter in most correlations was considered as an argument that other factors contribute to the efficiency of SEP acceleration. Kahler (2001) showed that correlations also exist between the SEP peak intensity and the pre-event intensity, and interpreted this as evidence that a pre-accelerated seed population increases the acceleration efficiency of a

CME shock. Gopalswamy *et al.* (2004) argued that CME interaction enhances SEP intensities.

The main and inevitable limitation of such statistical studies is that SEP intensities are generally measured at only one point. Its magnetic connection to the accelerator is not well known. It is often approximated by a Parker spiral. But this may not be true, as has been shown by event studies where SEPs reach the detector in transient interplanetary magnetic field (IMF) structures, *i.e.* interplanetary coronal mass ejections or ICMEs (Tranquille *et al.*, 1987; Torsti, Riihonen, and Kocharov, 2004; Malandraki *et al.*, 2005; Kahler, Krucker, and Szabo, 2011). Masson *et al.* (2012b) have shown recently that the majority of relativistic SEP events of solar cycle 23 were detected within or in the vicinity of ICMEs. These ICMEs stem from solar activity that occurred one or several days before the SEP event, so that the magnetic configuration had the time to expand and reach the Earth.

This paper presents a re-assessment of statistical relationships between the peak intensities (and fluences) of particle events (*i.e.*, near-relativistic electrons of tens to hundreds of keV and deka-MeV protons), and the parameters of the associated coronal activity (*i.e.*, the peak SXR flux of the flare and the speed and width of the CME). Two categories of IMF configuration guiding the particles through the IP space are distinguished: standard solar wind and ICMEs. All SEP events of solar cycle 23 (1997 – 2006) that occurred with flares of classes M and X[1] in the western solar hemisphere are considered. The data sets and analysis technique are described in Section 2. Section 3 presents the observational findings: the identification of SEP events within ICMEs and within the standard solar wind, together with the distributions of peak particle intensities (Section 3.1), rise times (Section 3.2), and connection distances to the parent flare (Section 3.3). In separate subsections we address the following statistical relationships: between the flares and CMEs (Section 3.4.1), between the SEP intensity (Section 3.4.2), and rise-to-peak fluence (Section 3.4.3), on one hand, and the parameters of the associated solar activity, on the other. The ICME category is discussed in more detail in Section 3.4.4 and the effect of the connection distance on the correlations in Section 3.4.5. Section 4 addresses the influence of observational bias and physical effects on the correlation between the intensity of deka-MeV protons and near-relativistic electrons and the parameters of the parent coronal activity.

2. Data Analysis

The data set for this statistical study is composed of SEP events between 1997 and 2006 (23rd solar cycle) associated with well-identified activity in the western solar hemisphere (flares at longitude $< 90°$), using the list of SEP events at energies above 25 MeV of Cane, Richardson, and von Rosenvinge (2010) based on IMP-8 and SOHO/ERNE data. Several events were excluded because of high background from a preceding particle event (typically when the two subsequent SEP events are less than 8 – 10 h apart). We excluded from the statistics also SEP events that occurred during a SOHO data gap. This leads to a data sample that contains 38 SEP events associated with X-class flares and 66 with M-class flares.

For the quantitative analysis of the proton data we use three complementary sets of observations: GOES 15 – 40 MeV data from the Ionising Particle ONERA DatabasE (IPODE) developed at the Office National d'Etudes et Recherches Aérospatiales (ONERA) in Toulouse,

---

[1]GOES X-ray classification in the 1 – 8 Å channel: M-class flares have peak flux that exceeds 10^{-5} W m^{-2}, whereas the X-class flares are 10 times more intense.

provided by D. Boscher. This database hosts GOES data that were carefully compared between simultaneously observing GOES spacecraft and corrected for evident outliers. Additionally we use the *Wind*/EPACT 19 – 28 MeV particle data available *via* the CDAWeb service,[2] reported there as preliminary browse data, and the SEP events in Cane, Richardson, and von Rosenvinge (2010). This yields a total of 81 SEP events observed by GOES, 96 by *Wind*/EPACT, and 104 from Cane, Richardson, and von Rosenvinge (2010). The three data sets from different instruments with different calibrations allow for consistency checks of statistical results. Energetic electron data are used as measured by the 38 – 53 keV and 175 – 315 keV energy channels of the EPAM experiment[3] aboard the *Advanced Composition Explorer* (ACE) spacecraft (Gold *et al.*, 1998).

A constant pre-event background was subtracted from the particle intensities. While determining the peak particle intensity, we sought for the maximum of the SEP events, avoiding late peaks that could be associated with energetic storm particle (ESP) events. An additional difficulty in estimating the intensity peak was the presence of several maxima in the time evolution. In such cases (denoted with *m* in the tables in the Appendix) we took the largest intensity maximum.

Data on flare size, times, and heliographic location were taken from the *Solar Geophysical Data* reports[4] compiled by NOAA. The CME speed is the projected one reported (as linear speed) in the CDAW catalog[5] (Yashiro *et al.*, 2004). The CME angular widths are taken from Cane, Richardson, and von Rosenvinge (2010), who estimated the angular width of each CME in the LASCO-C2 instrument field of view (heliocentric distance 2.5 – 6 solar radii). The complete event list and the information on the related parameters is given in the Appendix (Tables 4 – 6).

3. Observational Findings

3.1. Interplanetary Magnetic Field Configuration

In order to classify the SEP events into categories according to the magnetic field configuration guiding the particles from the Sun to the Earth, we compared the times of onset and rise of the SEP profiles with the start and end times of ICMEs reported by Richardson and Cane (2010). The time boundaries of the ICME were inferred there primarily from plasma and magnetic field data measured by the ACE spacecraft and are reported to the nearest hour. This catalog gives, together with different ICME characteristics, the time of the disturbance at Earth, the start and end times of the ICME at ACE (and occasionally at the *Wind* spacecraft). We shifted the ICME times measured at ACE (positioned at the Lagrangian L1 point) to the GOES orbit taking the reported ICME speed as constant over the distance between the two spacecraft. When the onset and rise of the SEP event was detected while the Earth was within an ICME, we consider that the particles propagated in a transient flux tube of an ICME. These SEP events are called 'ICME events' in the following. When the SEP onset occurred at least one day after the end of a previous ICME at the Earth and at least one day before the start of the next ICME, we consider that the particles propagated within

Table 1 Number of SEP events in the different IMF configurations with respect to the associated flare size.

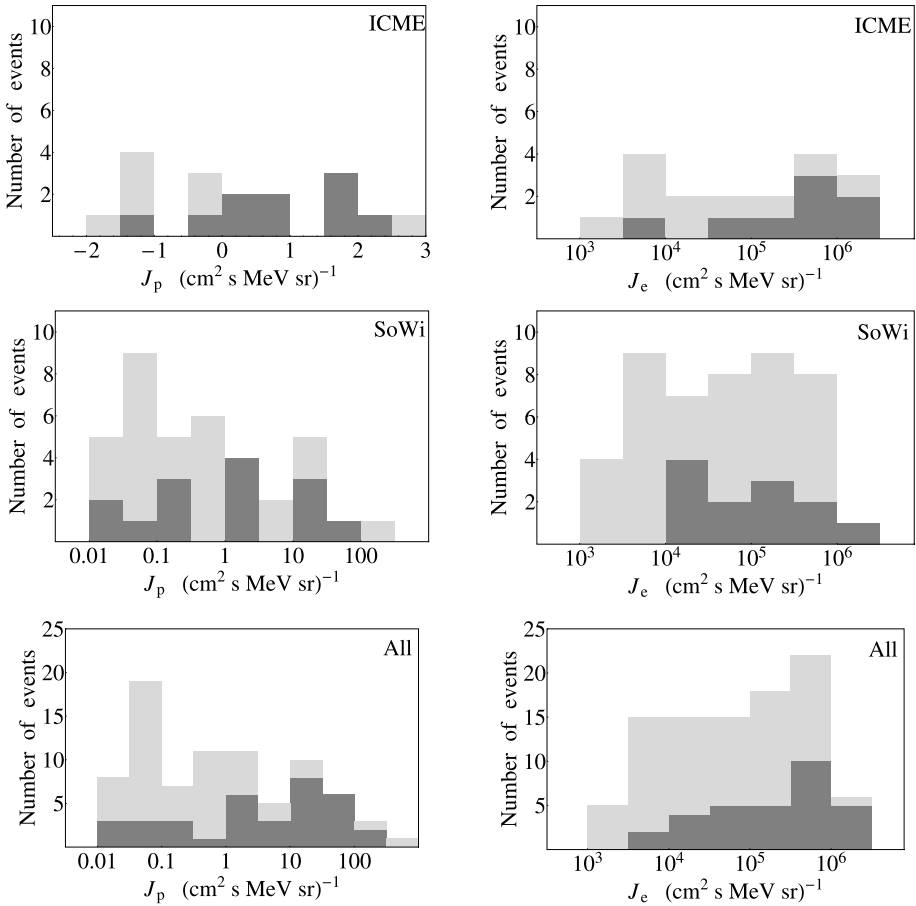| Flare size	IMF categories of SEP events		
	ICME	SoWi	All SEPs
Protons	GOES/*Wind*-EPACT/Cane, Richardson, and von Rosenvinge (2010)		
M-class	7/11/9	24/29/36	46/60/66
X-class	10/11/11	14/14/16	35/36/38
(X + M)-class	17/22/20	38/43/52	81/96/104
Electrons	ACE/EPAM 38 – 53 and 175 – 315 keV		
M-class	10	34	65
X-class	8	12	31
(X + M)-class	18	46	96

the standard solar wind. Those events are called 'SoWi events'. In the remaining events the IMF configuration is uncertain. In those cases the SEP may propagate in the solar wind, in the vicinity of the shock, in the sheath, or in disturbed interplanetary field lines behind the ICME, which may result from reconnection between the ICME and the ambient solar wind. Finally, the labels 'All'/'All SEPs' denote the complete set of SEP events, comprising the categories of ICME, SoWi, and the SEP events in the vicinity on an ICME (Tables 4 – 6 in the Appendix).

The distributions of the SEP events among the IMF categories and also with respect to the size of the associated flare (in GOES X-ray classification of the 1 – 8 Å channel) are listed in Table 1. On separate rows we give the number of SEP events associated with M-, X-, and (X + M)-class flares, respectively. The three proton instruments detected different numbers of SEP events related to M- and X-class flares (probably due to their different sensitivities). The three proton entries separated by slashes refer to the SEP events observed by GOES, *Wind*/EPACT, and from the catalog of Cane, Richardson, and von Rosenvinge (2010), respectively. The table shows that a significant number of SEP events are observed when the Earth is within an ICME, and that the ratio of ICME events to the total number increases with the importance of the parent activity: 29 % of the proton events associated with X-class flares belongs to the ICME events (*e.g.*, 10/35 cases observed by GOES), but only between 14 % and 18 %, depending on the data set considered, of the proton events accompanied by M-class flares. For electron events this ratio is 26 % for X-class flares and 15 % for M-class.

In the following figures we present statistical properties and correlations of the SEP events that are in general given as a comparative set of plots for the protons (on the left) and electrons (right) in the different IMF categories, namely ICME, SoWi, and All events. Unless stated otherwise in the text, the proton data in the figures are for the 15 – 40 MeV peak intensity measured by the GOES instrument, whereas the electron data are from the low energy channel of ACE/EPAM. Since the numbers of proton and electron events are slightly different (for a few SEP events there are proton but not electron data and vice versa), we carry on the analysis for both particle species separately.
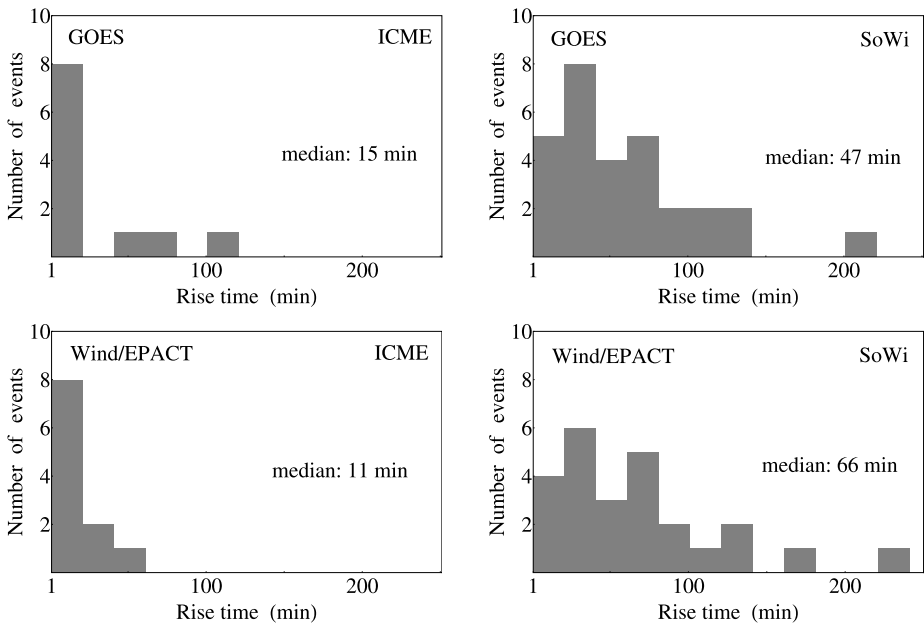
The distributions of the peak differential intensities of protons, J_p, and electrons, J_e, are given in Figure 1 in 'stacked form'. Dark shading shows SEP associated with X-class flares and light shading with M-class flares. The total distribution is the envelope of the two colored sections. The proton and electron plots in Figure 1 show essentially the same overall ranges of peak intensities in ICME events and SoWi events, both for electrons and protons. The details of the histograms show some differences: Proton distributions of the

Figure 1 Distributions of the proton (left) and electron (right) peak intensity for the different IMF categories of SEP events (proton data from GOES and electron data from low energy channel of ACE/EPAM). The number of SEP events in each category is given by the length of the corresponding color bar in each bin. SEP events associated with X-class flares are highlighted in dark gray color, whereas M-class associated SEP events are given in light gray.

entire data set and of the SoWi events peak at low differential peak intensities, whereas the protons of the ICME category and the electrons of both categories are more evenly distributed. There seems to be a tendency of a larger fraction of high intensity electron events in the whole population of SEP events, but a larger fraction of low intensity proton events. However, the differences of the distributions between ICME and SoWi events are not significant: A chi-square test shows that the ICME and SoWi intensity distributions can be drawn from the same parent distribution with a probability of 67 % for the protons and 98 % for the electrons, respectively.

The two IMF categories of SEP events (ICME and SoWi) show no conspicuous difference in event-averaged composition (*e.g.*, electron-richness, iron-richness, *etc.*, as identified for each event by Cane, Richardson, and von Rosenvinge, 2010).

Figure 2 Distributions of the GOES and *Wind*/EPACT proton rise times for the different IMF categories of SEP events (ICME in the left and SoWi in the right panels). The number of SEP events in each category is given by the length of the corresponding color bar in each bin.
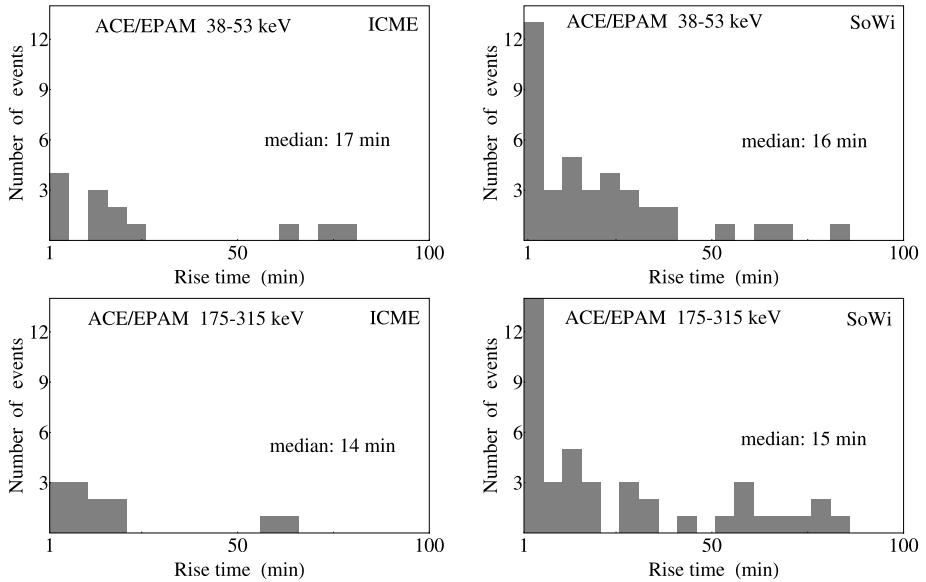
3.2. Rise Time

In order to investigate if the particle transport is different in the two IMF categories, we evaluated the rise times of the intensity profiles.[6] This is most easily done if the onset and peak of the profile are clearly defined. However, especially the intensity profiles of deka-MeV protons may be complex with fluctuations superposed upon a general rise or with a gradual flattening to a poorly defined maximum. The simple definition of the rise time as the time from start to maximum did not lead to consistent results for different instruments. A detailed discussion of rise time determinations is given in Posner (2007).

To determine the rise time of proton and electron time profiles, we used a method similar to Masson *et al.* (2012b): The particle intensity was first divided by the pre-event background. The logarithm of the normalized background intensity is hence zero. This logarithmic time profile was then again normalized to the first identified maximum or to the value at the first significant break of the slope of the profile. Usually the rise slows down during the event. The time for the second normalization was hence chosen such as to identify the fastest part of the rise phase. The estimated rise time is the time of the exponential rise of the profile as inferred from a linear least absolute deviation fit to the logarithmic profile be-tween the levels 0.2 and 0.8. The results are given in column (11) in Tables 4 and 5 in the Appendix.

We applied this method to the GOES and *Wind* proton data sets and obtained consis-tent results (given as histograms in Figure 2): Proton events in the ICME category have

---

[6]Estimating transport effects from rise times is valid under the assumption of a single, short in time particle injection.

Figure 3 Distributions of the ACE/EPAM low- and high-energy channel electron rise times for the different IMF categories of SEP events (ICME in the left and SoWi in the right panels). The number of SEP events in each category is given by the length of the corresponding color bar in each bin.

three times shorter rise times (median value and its deviation of 15 ± 6 min for GOES and 11 ± 7 min for *Wind* data) than SoWi events (median value of 47 ± 25 min for GOES and 66 ± 35 min for *Wind* data).

Rise times of the electrons, derived from the low-energy and high-energy channels of ACE/EPAM 5-min data, do not show a systematic difference between ICME and SoWi events (Figure 3). The median values of the rise times are 17 ± 13 min (ACE/EPAM $38-53$ keV) and 14 ± 7 min (ACE/EPAM $175-315$ keV) in the ICME category and 16 ± 12 min and 15 ± 14 min in the SoWi category. Although there are more electron events with longer rise times in the SoWi category than in the ICME category, there are also numerous electron events propagating in the solar wind with rise times less than 5 min (given with one bin in the plots), which decreased the median value of the rise time. To optimize the presentation, only electron events with rise times shorter than 100 min are included in the histograms (but all events are used to calculate the median rise time).

3.3. Connection Distance

Inspection of column (7) in Tables 4 and 5 suggests that the longitude distribution of the flares associated with the SEP events in the two IMF categories are different: The distribution is flat for the SoWi events, but peaks in the range $40°-80°$ for the ICME events. This difference can affect statistical relationships between the parameters of SEP events and the associated coronal activity in two ways. First, because of the broader distribution of projection angles, the projected CME speeds may be more strongly randomized in the SoWi sample than the ICME sample. Second, the distribution of angular distances between the IP field line through the Earth and the region of strongest particle injection in the corona is expected to induce a stronger dispersion of peak SEP intensities in the SoWi sample than the

ICME sample. Projection effects on CME speeds will be addressed in Section 3.4.1. Here we evaluate the effect of the connection distance on the SEP detection and peak intensity.

Ideally the connection distance is the angular distance between the footpoint of the IMF line through the Earth on the solar wind source surface and the footpoint in the low corona of the field line onto which the bulk of the SEPs is injected. Here we use the Parker spiral as a proxy of the IMF line and the flare longitude as a proxy of the coronal field line with the highest SEP intensity. We follow the common assumption of a spherical heliocentric source surface with radius $r_{SS} = 2.5\ R_\odot$. The longitude on the source surface of the Parker spiral through the GOES spacecraft at heliocentric distance $r_{GOES} = 214\ R_\odot$ is

$$\phi_{PS} = \frac{2\pi}{P\,V_{SoWi}}(r_{GOES} - r_{SS}), \tag{1}$$

with an averaged solar rotation period of $P = 26$ days. The solar wind speed, V_{SoWi}, is taken from the MTOF/PM sensor[7] of the CELIAS instrument aboard SOHO (Hovestadt *et al.*, 1995), and is the averaged value over a 6-h period before the particle onset time (see Tables 4–6). It is expected that SEPs are guided along field lines of different geometry within an ICME than in the solar wind. We nevertheless present the connection distance for the ICME category using the same formula as for the SoWi events, because the legs of the IP flux ropes are expected to be curved similarly to the Archimedian spiral by the combination of outward expansion and solar rotation (Marubashi, 1997; Vandas, Odstrčil, and Watari, 2002). The results are given in the last column of Tables 4–6 in the Appendix.

The distributions of connection distances for the different IMF categories are shown in Figure 4 (histograms), together with the peak particle intensity (filled and empty circles for the SEP events associated with flares of classes X and M, respectively). The median values and deviations for the connection distance of GOES protons[8] are $14° \pm 13°$ ($23° \pm 8°$ in absolute values) for the ICME events and $-5° \pm 19°$ ($14° \pm 11°$ in absolute values) for the SoWi events. For the electron events (ACE/EPAM low energy channel) we obtain $13° \pm 15°$ ($23° \pm 9°$ in absolute values) for the ICME events and $-5° \pm 20°$ ($18° \pm 14°$ in absolute values) for the SoWi events, respectively. All distributions cover a wide range of distances ($\pm 60°$) around the nominal connection longitude ($0°$), but the scatter is more pronounced for the SoWi events, which have (for GOES data set) 26/38 events (68 %) at connection distances above $30°$, as compared to 13/17 ICME events (76 %).

At first glance there is no evidence for a systematic decrease of peak particle intensity with increasing connection distance. Both IMF categories comprise events which are intense, even though the associated flare is far from the nominal connection longitude. The connection distance distributions of the peak intensities are in general flat. We note, however, that the SEP events of the SoWi category with large connection distances ($> 30°$) are preferentially accompanied by strong (X-class) flares. So if, as we will show in Section 3.4.2, stronger SXR bursts are associated with stronger SEP intensities, the over-representation of X-class flares in the remote SEP events does reveal a general trend of decrease of the peak particle intensity with increasing connection distance.

3.4. SEP Events and Associated Coronal Activity

Before investigating if and how the statistical relationship between SEP peak intensity and the parameters of the associated flare and CME depends on the IMF configuration, we ad-

---

[7]http://umtof.umd.edu/pm/crn/.

[8]For the *Wind*/EPACT proton data we obtain $22° \pm 13°$ ($20° \pm 8°$ in absolute values) for the ICME events and $-6° \pm 20°$ ($14° \pm 11°$ in absolute values) for the SoWi events.
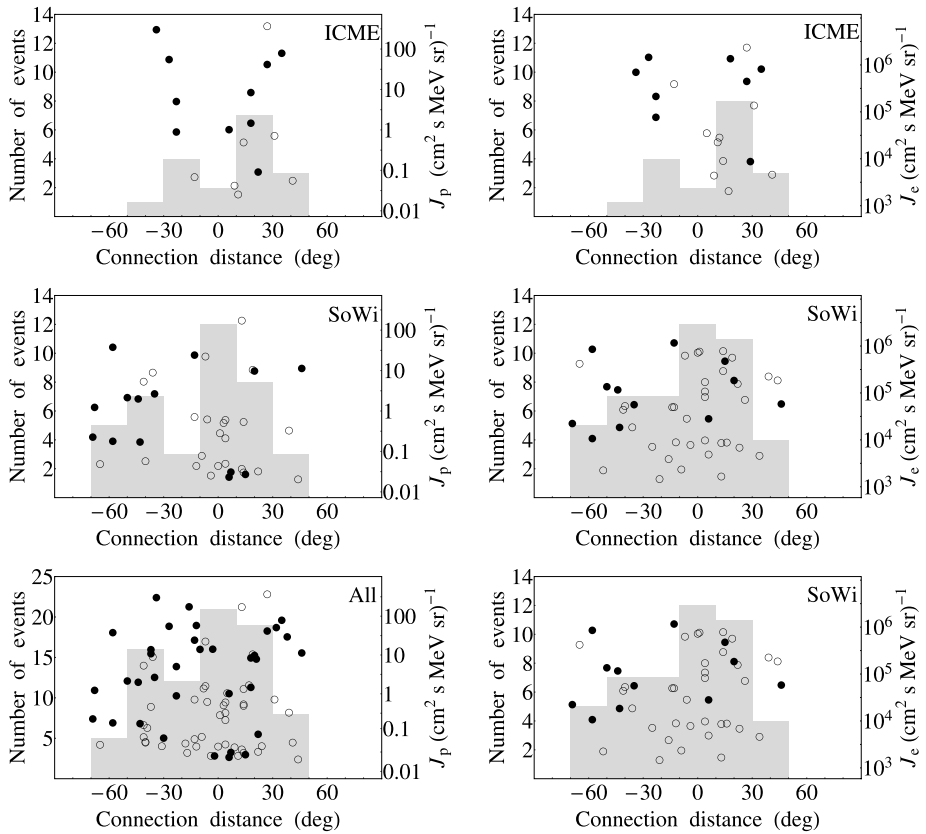
Figure 4 Distribution in connection longitude for different categories of SEP events. Overplotted are the SEP peak intensities for the GOES proton (J_p, left) and ACE/EPAM electron (J_e, right) data. Filled and open circles denote the SEP events associated with X-class and M-class flares, respectively.

dress the correlation between the peak soft X-ray flux (I_{SXR}) and the projected CME speed (V_{CME}). This is necessary to see if the parent solar activity is similar in the two event categories or if selection effects are important. Some correlation is expected because of the general experience, termed the big flare syndrome (Kahler, 1982b), that solar events that are important with respect to one parameter are likely important with respect to other parameters, too.

3.4.1. Correlations Between Flare and CME Parameters in Different IMF Categories

We present the log–log scatter plots of I_{SXR} *vs.* V_{CME} in different IMF categories. For the flare/CME events associated with proton events observed by GOES they are shown in Figure 5, and for the events accompanied by electrons (ACE/EPAM low energy channel) in Figure 6. There is an overall correlation for the entire event sample for both particle species, which shows that on average faster CMEs accompany stronger SXR bursts (correlation co-
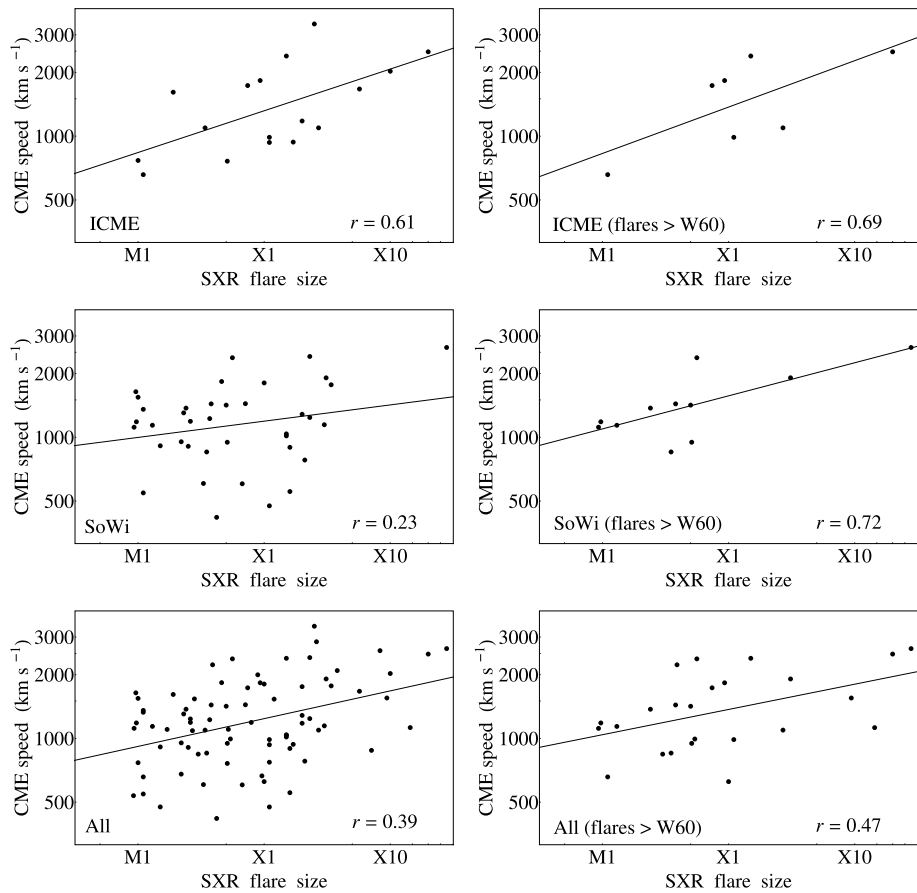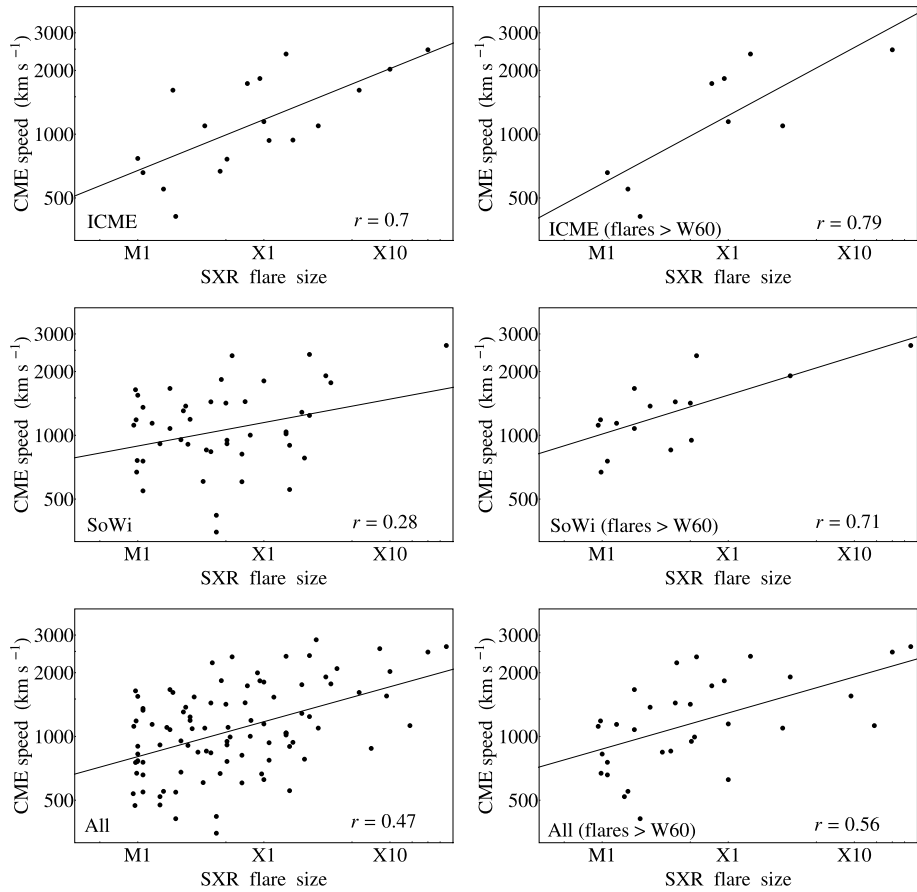
Figure 5 Scatter (log–log) plots of SXR flare size *vs.* CME speed for different IMF categories of GOES proton events (left) and for a subset of these events associated with flares at longitudes $> W60°$ (right).

efficient[9] of $0.39 - 0.47$). This was known before: Vršnak, Sudar, and Ruždjak (2005) gave a value of 0.35 (with a statistical significance larger than 99.99 % by the t-test), and Yashiro and Gopalswamy (2009) gave a value of 0.5.

In order to assess the significance of the correlations, we performed a simple error analysis using the 'bootstrap' method (Wall and Jenkins, 2003). It consists of drawing repeatedly, out of a sample of N events, N events at random, and computing the correlation coefficient for this sample. This is repeated 1000 times, and the average value of the sample of correlation coefficients and its standard deviation are calculated. For all correlation coefficients calculated in the present work, the standard deviations will be given according to this method.

The left column of Figures 5 and 6 suggests a difference between the behavior of the SEP events in the two IMF categories, with a stronger correlation between $\log I_{SXR}$ and

---

[9]Note that the r^2-values of the correlation coefficients found in the present study (and also in earlier work) are usually $r^2 \lesssim 0.5$.

Figure 6 Scatter (log–log) plots of SXR flare size *vs.* CME speed for the different IMF categories of ACE/EPAM electron events (left) and for a subset of these events associated with flares at longitudes > W60° (right)

log V_{CME} in the ICME events, $0.61 - 0.70$, as compared to the SoWi events (about twice as low, $0.23 - 0.28$). The difference is statistically significant, see Table 2.

The difference in the two IMF categories is of course unexpected, because there is no physical reason why the correlation between two manifestations of coronal activity should depend on the IMF structure. We therefore look for observational biases. An obvious one is the projection effect (Burkepile *et al.*, 2004; Vršnak *et al.*, 2007), which will decrease the CME speed, measured in projection onto the plane of the sky.

In order to test this, we calculated the correlation coefficients for different sub-samples (Table 2). A closer inspection of the left column of plots in Figures 5 and 6 shows that the SoWi events associated with fast CMEs, as seen in the upper envelope of the scatter plot, seem to follow a similar (*i.e.* stronger) correlation as the ICME events. This trend is confirmed when we removed all SEP events from the sample associated with projected CME speed below 600 km s^{-1}. This brings the correlation coefficients slightly closer to each other (see the values in Table 2).

Table 2 Linear correlation coefficients (with standard deviations) between the log I_{SXR} and log V_{CME} for proton and electron data set in the different IMF categories.

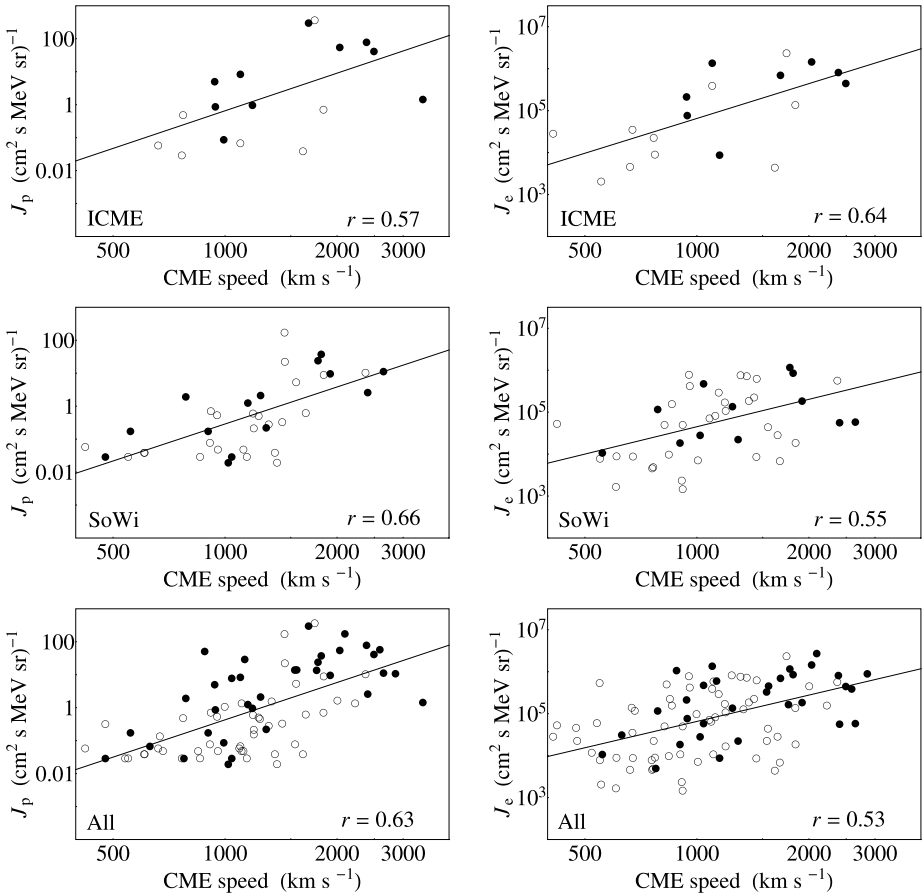| SEP event sub-samples	IMF categories of SEP events		
	ICME	SoWi	All SEPs
Protons	GOES $15-40$ MeV		
No event restriction	0.61 ± 0.14	0.23 ± 0.16	0.39 ± 0.09
$V_{CME} > 600$ km s^{-1}	0.61 ± 0.14	0.29 ± 0.18	0.38 ± 0.09
Flares $>$ W60°	0.69 ± 0.36	0.72 ± 0.21	0.47 ± 0.15
Electrons	ACE/EPAM $38-53$ keV		
No event restriction	0.70 ± 0.12	0.28 ± 0.14	0.47 ± 0.08
$V_{CME} > 600$ km s^{-1}	0.65 ± 0.16	0.36 ± 0.16	0.40 ± 0.09
Flares $>$ W60°	0.79 ± 0.14	0.71 ± 0.15	0.56 ± 0.10

In order to avoid projection effects due to events close to the disc center[10] we then removed all SEP events associated with flares at longitudes below 60°. The right column of plots in Figures 5 and 6 shows that this improves the correlations for all IMF categories of events. The largest increase in the correlation coefficient is for the SoWi events (compare the middle plots), but the standard deviation also increases due to the smaller number of events (Table 2). The change is less for the ICME events and only a slight increase is found for the entire data set (denoted with 'no event restriction' in Table 2). Burkepile *et al.* (2004), considering the correlation between the kinetic energies of CMEs and SXR peak flux, also showed that the correlation coefficient increased if one considers only limb events.

In summary, the poor correlation between the projected CME speed and the peak SXR flux for the SoWi event sample can be ascribed to randomization of an existing relationship by the broad variety of flare longitudes, and to a lesser extent to events with slow CMEs. Hence projection effects play a role in the determination of CME speed. This role is apparently more important in the SoWi event sample, where the flares happen to be distributed over a broader range of longitudes than in the ICME sample. It does not seem to be possible to avoid this problem with the data sets at hand, since a restriction to limb events increases the correlation coefficient, but also its uncertainty. Attempts to empirically correct the CME speed for projection effects do not seem to increase the correlation with the SXR flux (Yeh, Ding, and Chen, 2005). The actual correlations of SEP parameters with CME speeds are expected to be higher than the values we find from our data set. This applies especially to the SoWi events. On the other hand, the broader range of longitudes may also affect the peak particle intensity, in line with our previous finding that the range of connection distances is broader in the SoWi category than in the ICME events.

3.4.2. Statistical Relationships Between SEP Peak Intensities and Parameters of the Associated Solar Activity

In this section we search for statistical relationships between the peak SEP intensity (J_{max}) and parameters of the associated coronal activity, namely the peak SXR flux and the CME projected speed. Only the scatter plots for the GOES proton (Figure 7) and ACE/EPAM electron (Figure 8) data sets are shown, for the ICME, SoWi events and the entire sample. Linear correlation coefficients r between the logarithmic quantities are given in each frame.

---

[10]Note that five of the eight events in the SoWi category with projected speed below 600 km s^{-1} occurred near the central meridian.

Figure 7 Scatter (log–log) plots of the peak proton (J_p, left) and electron (J_e, right) intensity *vs.* the CME speed for different IMF categories of SEP events.

The logarithms of J_p and J_e show similar correlation coefficients with I_{SXR} and V_{CME} in the range $0.40 - 0.63$ for the entire event sample (see the bottom panels of Figures 7 and 8). Differences arise when the two IMF configurations are considered: While the correlations of log J_{max} with log V_{CME} are similar for ICME and SoWi events (Figure 7), the correlations with log I_{SXR} differ (Figure 8). Peak particle intensities are more strongly correlated with I_{SXR} than average in the ICME events, and are only weakly correlated in SoWi events. The difference is about a factor of two for the protons, and six for the electrons. The same results are found when the start-to-peak fluence, *i.e.*, the time-integral of the background-subtracted SEP intensity until the peak time, is used instead of the peak intensities.

As done previously (Section 3.4.1) the statistical uncertainties of the correlation coefficients are evaluated using the 'bootstrap' method. As a consistency check, we calculated the average value of each correlation coefficient, based on 1000 random selections. This value differs only less than 5 % from the value reported in Figures 7 and 8, drawn from the complete set of measured points. It is the latter correlation coefficients that are listed in Table 3 for the GOES and ACE/EPAM low energy channel data sets, together with the error estimates. The number of events in each SEP group is also given. Within the estimated
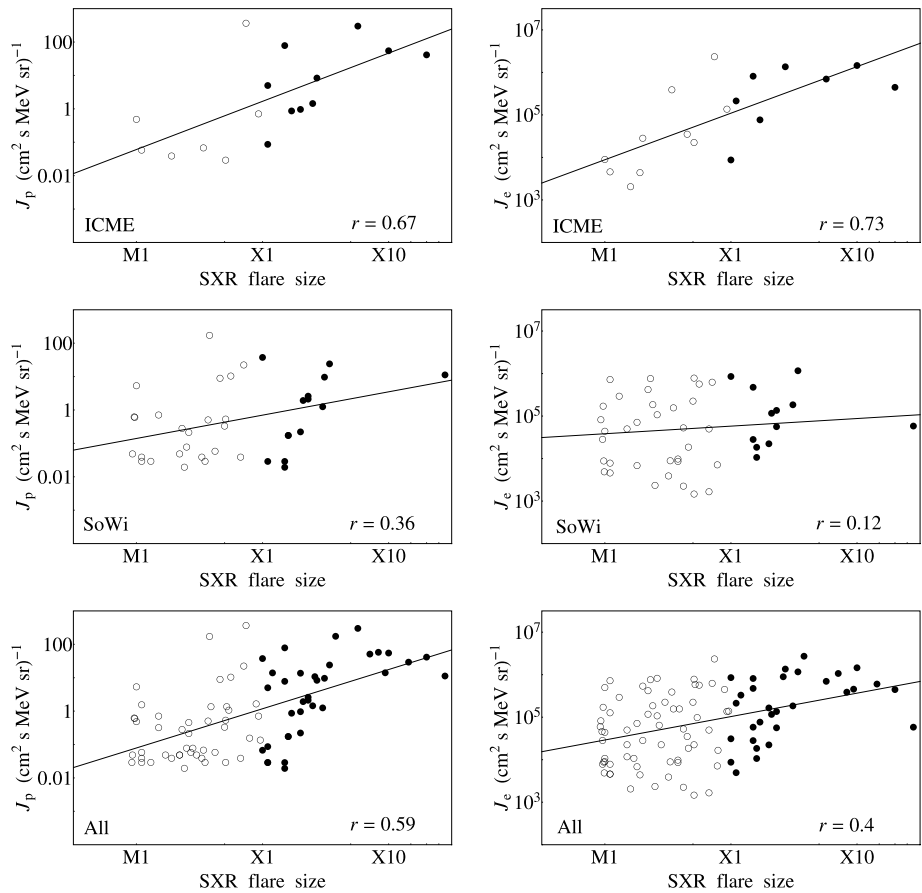
Figure 8 Scatter (log–log) plots of the peak proton (J_p, left) and electron (J_e, right) intensity *vs.* the soft X-ray flare size for different IMF categories of SEP events.

errors the correlation coefficient between J_{max} and V_{CME} is the same for ICME and SoWi events. It is also similar to the correlation between J_{max} and I_{SXR} for the ICME events. All these correlation coefficients are statistically higher than that between J_{max} and I_{SXR} for the SoWi events. The weak correlation of $\log J_{max} - \log I_{SXR}$ in the SoWi category is statistically significant result compared to the higher correlation found in the ICME category. The correlation coefficients drawn from the different data sets are consistent (see Table 3).

Given the discussion of the $I_{SXR} - V_{CME}$ correlation in Section 3.4.1, different correlations in the ICME and SoWi event categories may be biased due to different longitude distributions of the flare/CME events in the two categories. We therefore investigate if and how this bias also influences the correlations of J_{max} and the parameters of the coronal activity. For this we calculated the corresponding correlation coefficients of J_{max} with I_{SXR} and V_{CME} in the different IMF categories and for particle events associated with flares beyond certain longitude threshold. The results are summarized in Table 7 (in the Appendix), where the first row in each section is taken from Table 3 to facilitate the comparison. The trends for the different correlation coefficients are presented in Figure 9. The restriction to limb events ($> 60°$), however, reduces the number of events in each category to less than half of the

Table 3 Linear correlation coefficients of log J_{max} and log I_{SXR}, log V_{CME} and angular width (AW) for the different IMF categories.

| Correlation log J_{max} with:	IMF categories of SEP events		
	ICME	SoWi	All SEPs
Protons	GOES 15 – 40 MeV		
log I_{SXR}	0.67 ± 0.13	0.36 ± 0.13	0.59 ± 0.07
log V_{CME}	0.57 ± 0.15	0.66 ± 0.07	0.63 ± 0.05
AW	0.52 ± 0.18	0.23 ± 0.13	0.29 ± 0.10
Number	17	38	81
Protons	*Wind*/EPACT 19 – 28 MeV		
log I_{SXR}	0.71	0.41	0.62
log V_{CME}	0.73	0.68	0.68
AW	0.58	0.28	0.37
Number	22	43	96
Protons	Cane, Richardson, and von Rosenvinge (2010) > 25 MeV		
log I_{SXR}	0.86	0.31	0.61
log V_{CME}	0.68	0.55	0.61
AW	0.69	0.22	0.33
Number	20	52	104
Electrons	ACE/EPAM 38 – 53 keV		
log I_{SXR}	0.73 ± 0.10	0.12 ± 0.11	0.40 ± 0.08
log V_{CME}	0.64 ± 0.14	0.55 ± 0.09	0.53 ± 0.07
AW	0.48 ± 0.14	-0.09 ± 0.12	0.09 ± 0.10
Number	18	46	96
Electrons	ACE/EPAM 175 – 315 keV		
log I_{SXR}	0.74	0.31	0.57
log V_{CME}	0.63	0.63	0.59
AW	0.56	0.05	0.22
Number	18	46	95

original size and increases the uncertainty. Hence, due to the small number of events for this sub-sample, selection effects may play a role.

In general, the correlation log J_{max}–log V_{CME} stays the same within the uncertainties when we consider different subsets of limb events (compare the upper panel of plots in Figure 9). For the GOES protons, associated with flares at longitude $> 60°$, we find no statistically significant difference in log J_p–log V_{CME} (see the upper left plot in Figure 9): The increase of the correlation coefficient for ICME events to 0.76 ± 0.22 (from the previous value of 0.57 ± 0.15) is within the uncertainties, and there is practically no change in the correlation for the SoWi events (0.65 ± 0.14 compared to the previous value of 0.66 ± 0.07). However, we obtain a statistically lower correlation log J_e–log V_{CME} in the SoWi category, 0.14 ± 0.28 (see the upper right plot), but only when limb events $> 60°$ are considered (and not for $> 50°$ for example), so selection effects may be responsible for this result.

For the correlation log J_{max}–log I_{SXR} we find different trends for the two particle species (lower panel of plots in Figure 9). For the protons, the factor of two difference in the log J_p–log I_{SXR} correlation between the two IMF categories is no longer present for the limb events. Namely, we obtain 0.51 ± 0.34 for the ICME events and 0.54 ± 0.17 for the
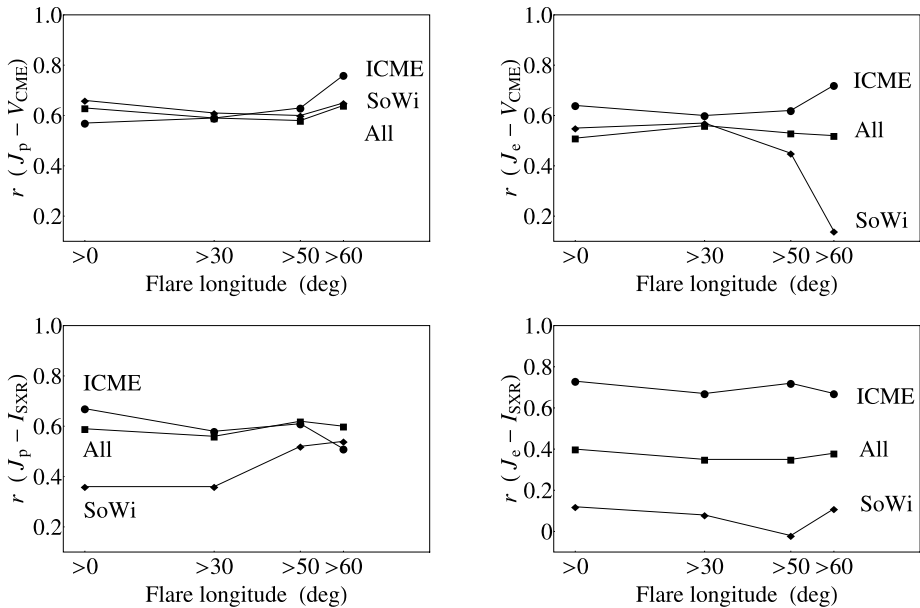
Figure 9 Trends for the correlation coefficients of the particle intensity (J_{max}) with V_{CME} and I_{SXR} for sub-samples of SEP events associated with flares at longitude above certain threshold. Dots, diamonds, and squares denote ICME events, SoWi and All SEP events, respectively.

SoWi events (see the lower left plot in Figure 9). For the ACE/EPAM low energy channel electron data, however, we still find statistically significant difference in the correlations $\log J_e - \log I_{SXR}$ between the two IMF categories (see the lower right plot in Figure 9). Namely, the correlation coefficient in the SoWi category, 0.11 ± 0.28, is lower than that in the ICME category, 0.67 ± 0.18, within the uncertainties.

We conclude that SEP events associated with flares close to disc center could be the main observational artifact that weakens the correlation of the proton intensity with the I_{SXR} for the SoWi events. For the electron events propagating in the solar wind another explanation is needed.

Finally, we consider the correlation between $\log J_{max}$ and the linear value of the angular width (AW) in the two IMF categories. As can be seen from Table 3, the correlation with the angular width is similar in behavior to that of the I_{SXR}, and not with the V_{CME}. Namely, the correlation coefficients for the protons (electrons) for the SoWi events are roughly twice (five times) as weak compared to those for the ICME events.

3.4.3. Start-to-Peak Fluence

A measure of the total number of particles detected by the spacecraft is the total fluence, which is the time-integrated particle intensity. Since some SEP events are followed by ESP events accelerated at a shock near the Earth, the end of an SEP event may be hidden and total fluence cannot be determined. We made an attempt to evaluate the fluence between the onset and peak of the event, by time integrating the (background-subtracted) particle profile. We will refer to this quantity as fluence (Φ) henceforth.

Essentially the same ranges of values for the fluence are found in ICME and SoWi events, both for electrons and for protons. The median values of the logarithm of proton fluence
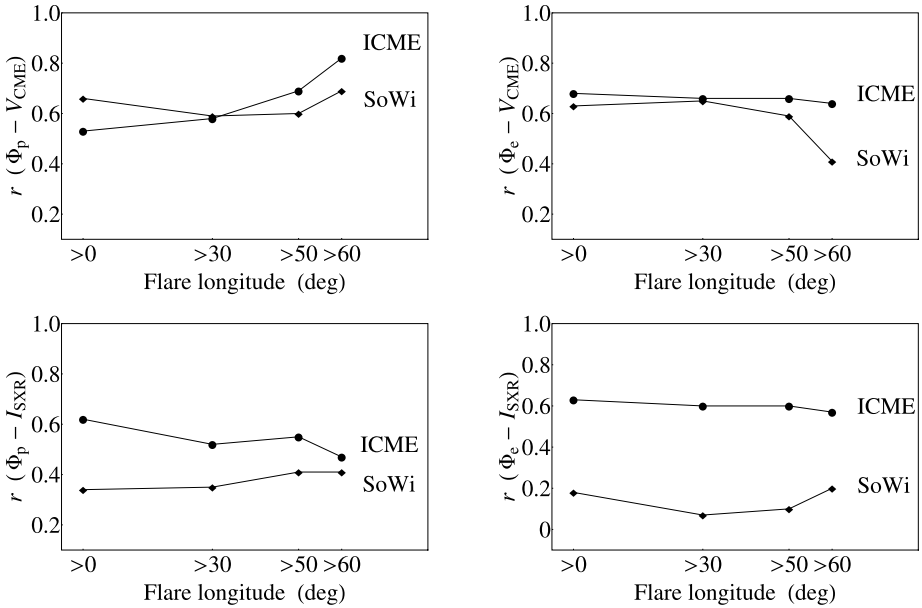
Figure 10 Trends for correlation coefficients of the fluence (Φ) with V_{CME} and I_{SXR} for sub-samples of SEP events associated with flares at longitude above certain threshold. Dots and diamonds denote ICME events and SoWi, respectively.

for the GOES data set are 3.8 ± 1.6 for ICME events and 3.3 ± 1.3 for SoWi events.[11] For the electron data, the median value of the logarithm of the electron fluence[12] for the ACE/EPAM low (high) energy channel is 8.6 ± 0.9 (7.4 ± 1.2) for the ICME events and 8.2 ± 0.9 (6.5 ± 1.0) for the SoWi ones. The values for the electron fluence were calculated after smoothing the data over 25 min.

For completeness, we investigated the correlation of the fluence with the I_{SXR} and with the CME parameters (see Table 8 in the Appendix). The correlation coefficients for the fluence are comparable to those of the particle intensity (Table 3) within the error bars. When we consider limb events (Figure 10), we obtain similar trends for the fluence as for the particle intensity (Figure 9). The fluence trends and the error estimates are summarized in Table 9 in the Appendix.

3.4.4. A Closer Look at the ICME Events

We considered so far ICME events as a well-defined category (in total we have 22 events; see Table 4). But one must actually envisage two physical scenarios: If particles accelerated in the corona are released into the legs of the ICME connected to the Earth, the SEP propagation is expected to be favored. This is probably the case when the flare and CME associated with the SEP event occur close to the footpoints of the ICME. If they occur far away, the ICME may actually shield the Earth from the SEP. In this case the ICME should

---

[11]Proton fluence could not be estimated for three events in the SoWi category.

[12]Electron fluence could not be estimated for one (four) events in the ICME (SoWi) category.

weaken the relationship between the SEP peak intensity and the parameters of the coronal activity. In order to check which of these scenarios applies, we compared the active region (AR) of the flare associated with the SEP event with the AR of the flare associated with the CME that gave rise to the ICME.

The number of ICMEs that come clearly from the same AR or at least from the same group of ARs as the SEP event is 16/22, where 10/16 of the SEPs are X-class associated events and 6/16 are related to M-class flares. There are three uncertain associations and three cases where the ARs of the SEP-associated flare and the ICME associated flare are not the same. Nevertheless, the majority of the SEP events, arriving inside (and presumably also propagating along the field lines of) the ICME, come from the same AR (13/22) or from the same group of ARs (3/22) as the ICME. It is hence to be expected that the SEP are directly released into the magnetic flux tube of the ICME, which is still magnetically connected to that AR.

Restricting the ICME sample to these 16 cases where the ICME and the SEP-associated activity come from the same AR (or group of ARs), and using *Wind*/EPACT data that comprise more events than the GOES data set, we obtained (log–log) correlation coefficients between J_p and I_{SXR} of 0.81 ± 0.08. There is a slight increase compared with 0.71 ± 0.10 for the complete set of ICME events in Table 3, but it is within the uncertainty estimate. The correlation coefficient of J_p with V_{CME} does not show a significant improvement, *i.e.*, for the 16 ICME events we obtained correlation coefficient of 0.77 ± 0.08 (compared to 0.73 ± 0.08 for the whole ICME group). Only 12 of these 16 ICME events from the same AR or cluster of ARs have electron intensities detected by ACE/EPAM. The corresponding (log–log) correlation coefficients of J_e are 0.64 ± 0.14 with I_{SXR} (compared to 0.73 ± 0.10 for the whole sample). The difference is not statistically significant, and there is no change in the correlation coefficient with V_{CME}, 0.65 ± 0.15 (compared with 0.64 ± 0.14).

In summary, we find an increase in the J_p–I_{SXR} correlation, a decrease in the J_e–I_{SXR} correlation, both within the error margins, and practically no change with the V_{CME} for both particle species. Due to the large uncertainties, the difference of the subset of ICME events and the entire ICME group is not statistically significant. Hence, proton propagation could be favored in the ICME, a trend that is supported by the faster rise times found for ICME events. Electrons from the same AR as the ICMEs show no trend of increased correlation with the parent activity. They also have similar rise times in both IMF configurations.

3.4.5. The Effect of the Connection Distance on the Correlations

We now compare the correlation coefficients for particle events around the best connection longitude (Section 3.3), referred to as inner events, with those farther away, outer events, for both IMF categories. The ICME and SoWi events are divided into inner and outer by the absolute value of the median connection distance for each IMF category. For the *Wind*/EPACT protons we have $20°$ for the ICME and $14°$ for the SoWi events, whereas for the ACE/EPAM electrons we have $23°$ and $28°$, respectively. The results (see Table 10 in the Appendix) have large error bars. The only significant effect is a better correlation of J_e with V_{CME} for the inner SoWi electrons than for the outer. No such trend is found for the protons. The observed difference in the correlation coefficients of J_{max} with I_{SXR} between the ICME and SoWi events cannot be explained by a mere longitude spread (inner/outer events) around the best nominal connection within the same IMF category. Another effect needs to be present.

4. Discussion

4.1. Summary of Observational Findings

The results of the statistical study of SEP events of solar cycle 23 associated with flares of class M or X in the western solar hemisphere are summarized as follows:

i) A significant number of SEP events (about 20 % – 17/81 GOES proton events and 18/96 ACE/EPAM electron events) were detected while the Earth was immersed in an interplanetary coronal mass ejection. This means that these deka-MeV protons and near-relativistic (tens to hundreds of keV) electrons were guided along transient interplanetary field lines, instead of the Parker spiral of the nominal solar wind.

ii) SEP events are relatively more often detected within ICMEs when the associated flare is of class X (10/35, 29 %) than of class M (7/46, 15 %).

iii) The peak intensities of electrons and protons cover a similar range for SEP events detected within ICMEs and in the standard solar wind. Indications of different peak intensity distributions in the two event categories are seen for protons, but they are not statistically significant. No such indication is seen for electrons.

iv) The proton profiles have a median rise time shorter (by a factor of three) within ICMEs than in the solar wind. The start-to-peak proton fluences of the two IMF categories are similar.

v) Contrary to protons, electrons have similar distributions of rise times in ICMEs and in the solar wind. They also have similar start-to-peak fluences in the two IMF categories.

vi) The longitudes of the parent active regions of the SEP events cluster around the nominal Parker spiral with some scatter for the ICME events, but have a very broad distribution for the events detected in the solar wind. There is no evident dependence of the peak intensity of protons or electrons on the connection distance.

vii) The underlying relationship between flares and CMEs (*i.e.*, between peak SXR flux and CME speed) is stronger for ICME events ($r = 0.61 - 0.70$) and weaker for SoWi events ($r = 0.23 - 0.28$). The weak correlation is ascribed to the randomization of the projected CME speed in the SoWi category. We conclude that there is a stronger intrinsic correlation between SXR peak flux and CME speed in the two IMF categories. The correlation for the entire event sample ($r = 0.39 - 0.47$) is comparable to previous reports.

viii) The correlation of SEP peak intensities J_{max} with the peak flux of the associated soft X-ray burst, I_{SXR}, and the speed of the associated CME, V_{CME}, depends on the IMF configuration:

- On average over all events, the correlation coefficients of $\log J_{max} - \log I_{SXR}$ and $\log J_{max} - \log V_{CME}$ are comparable, with values in the range $0.6 - 0.7$ for the protons and $0.4 - 0.6$ for the electrons.
- The correlation $\log J_p - \log I_{SXR}$ is twice as high in SEP events detected within ICMEs as for SEP events in the solar wind. The difference disappears when the sample is restricted to limb events.
- The correlation $\log J_e - \log I_{SXR}$ is about six times higher for the entire ICME sample and also for limb events as for SoWi sample.
- The correlation $\log J_{max} - \log V_{CME}$ is similar in both event categories and particle species.
- The above statements are valid for the correlations of the rise-to-peak fluence with the parent coronal activity.

4.2. The IMF Configuration of SEP Events

The occasional detection of SEP events within ICMEs is a well-known phenomenon. ICMEs provide an evident explanation why fast rising SEP events are occasionally observed in association with activity in the eastern solar hemisphere (Richardson, Cane, and von Rosenvinge, 1991). These authors estimated that about 15 % of SEP events from the eastern solar hemisphere have a rapidly rising intensity profile and showed that this may be due to propagation within an ICME. The percentage found in the present study for the SEP events from the western solar hemisphere (*i.e.*, 20 % arrive within ICMEs) is similar.

The fraction of GOES SEP events detected within ICMEs increases with the flare size. Such trend is also found by a relativistic proton event study. Masson *et al.* (2012b) showed that 7/10 relativistic SEP events of solar cycle 23 occurred within or in the vicinity of ICMEs. The associated flares ranged from X5.7 to X14 (with the exception of one behind-the-limb event). The numbers are not directly comparable, because the events in the neighborhood of ICMEs are excluded from the ICME events in the present study. Nonetheless there appears to be a trend that the more energetic the flare associated with a particle event, the greater the likelihood to detect the SEP within or in the vicinity of an ICME. This probably reflects the fact that on the one hand the ICME rate is enhanced in periods of high activity (Richardson and Cane, 2010), and that on the other hand strong flares (Bai, 1987; Sammis, Tang, and Zirin, 2000) and fast CMEs (Wang and Zhang, 2008) preferentially occur in a small number of highly active regions.

We found no significant evidence that the SEP intensity distributions differ between ICME events and SoWi events. Also the start-to-peak fluence distributions are similar. However, ICME events display on average faster rises in the proton profiles than SoWi events. This is consistent with the reported long scattering mean free paths of energetic protons in ICMEs (Tranquille *et al.*, 1987; Torsti, Riihonen, and Kocharov, 2004). No such effect is seen for the electrons. This is the first time, to our knowledge, that such a comparison is carried out.

4.3. IMF Configuration and the Correlation between SEP Parameters and Solar Activity

A number of studies in the literature report overall, but noisy, correlations between the logarithms of SEP proton (J_p) intensity and the logarithms of SXR peak flux and/or CME speed. The correlation coefficients between $\log I_{SXR}$ and $\log J_p$ at deka-MeV energies were found near 0.5 (36 events in 1973–1979) from Kahler (1982a) or 0.4 (25 events in 1996–2001) from Gopalswamy *et al.* (2003). Higher correlation coefficients were reported with $\log V_{CME}$: 0.7 (71 events in 1986–2000) from Kahler (2001) or 0.6 from Gopalswamy *et al.* (2003). Cane, Richardson, and von Rosenvinge (2010) report the same value of 0.6 for the correlation with $\log I_{SXR}$ and $\log V_{CME}$ (≈ 100 events in 1997–2006). No estimate of the uncertainty of these correlation coefficients was given.

The overall correlations found in the present study between the logarithms of peak SEP intensity and SXR peak flux on the one hand, CME speed on the other, are comparable, with correlation coefficients in the range of 0.4–0.7 for both electrons and protons and a statistical uncertainty of about ± 0.07. The entire event sample does not support the claim (Gopalswamy *et al.*, 2003) of a higher correlation coefficient of SEP peak intensities with CME speed than with soft X-ray flux. Our result agrees in this respect with that of Cane, Richardson, and von Rosenvinge (2010) who reported a value of 0.6.

A finer distinction between the two IMF categories – the standard solar wind and ICMEs – is subject to caution, because the solar wind sample is more strongly affected

by projection effects on CME speeds (due to larger variety in longitudes of the associated flare) and variable connections between the parent solar activity and the Earth-connected IMF line. We find no difference between the correlation coefficients $\log J_{max} - \log V_{CME}$ in the two IMF categories, but a marked difference for the correlation $\log J_{max} - \log I_{SXR}$. This is true for both protons and electrons. For electron events propagating in the solar wind there is virtually no correlation between $\log J_e$ and $\log I_{SXR}$, while it is significant in ICME events. The behavior of protons is less clear: They show low correlation between $\log J_p$ or peak fluence and $\log I_{SXR}$ for the entire SoWi sample (as the electrons), but the difference disappears when the sample is restricted to limb events. However, it is uncertain if the latter relationship points to a real physical effect due to the small event sample involved and large error bars on the correlation coefficients. We conclude that the IMF structure likely affects the correlation between peak particle intensity and peak SXR flux, and that this difference comes mostly from the fact that the ICME events covers a narrower range of flare longitudes and connection distances than the SoWi events.

4.4. A Tentative Interpretation

The correlation between $\log J_{max}$ on the one hand, and $\log V_{CME}$ or $\log I_{SXR}$ on the other, is not suited to discriminate clearly between CME-related and flare-related SEP acceleration processes. Statistical relationships do exist, but they appear to be strongly dependent on the location of the parent activity in the corona and the observer. Furthermore, the statistical relationship between SXR peak flux and CME speed is rather strong itself. This agrees with the recent findings of close relationships between CME kinematics and energy release in flares (Zhang *et al.*, 2001; Bein *et al.*, 2012). Irrespective of the acceleration agent and mechanism, particles are released from the acceleration region in a direction that can cover a range of angular orientations and also be event-dependent. If it scatters around the normal to the photosphere, the direction of maximum particle intensity will be in some range around the longitude and latitude of the flare, and may well vary during the event (*cf.* Masson *et al.*, 2012a). Since they are detected at the Earth, the particles reach the magnetically well-connected IMF line, which is likely a Parker spiral on average, but again with a broad scatter (*e.g.*, Smith, 2008). During their interplanetary travel the particles are also subject to pitch-angle scattering due to the magnetic inhomogeneities. All these effects will introduce additional blurring in the correlation between the particle intensity and the parameters of the parent activity. We consider in more details the IP transport and the connection distance.

The estimation of rise time in the present study is used as a proxy for the IP transport. We find the rise times of proton profiles scatter over a much broader range in SoWi events than in ICME events. This suggests a broader variation of mean free paths with respect to pitch-angle scattering in the SoWi events. One then expects that a given peak intensity at injection will be smeared out into a range of peak intensities at 1 AU, depending on the scattering conditions encountered. The much lesser dispersion of rise times in the ICME events is consistent with the long mean free paths found in some earlier studies. Then, any existing correlation between the peak SEP intensity and the flare strength will be better preserved in ICME events than in SoWi events. But while this argument works for protons, it does not for electrons: Electrons, like protons, show stronger correlation with SXR flux in ICME events than in SoWi events, but have similar (median values for the) rise times in the two IMF categories. So the interplanetary propagation of the SEP cannot be the only reason for the different correlations with peak SXR flux.

The other difference between the ICME and SoWi samples is in the connection distance. We found that both electrons and protons tend to come from activity that is closer to the optimal magnetic connection with the Earth in ICME events than in SoWi events.

Flare-related particle acceleration occurs in small volumes within or around an active region. The coronal magnetic field guiding the particles from the acceleration site to the magnetically well-connected field lines is essential for the detection of flare-related particles. The broad scattering of connection distances observed in SoWi events then suggests a stronger blurring than in ICME events, and an ensuing loss of correlation between J_{max} and I_{SXR}. The broad range in connection distances combined with a spread in injection angles of the SEPs may also be responsible for the flat distribution of the particle intensity with connection distances (see Figure 4).

A CME shock is a rather extended accelerator and is expected – at least in simple scenarios – to inject particles into a broad cone of interplanetary field lines. This makes the correlation of the peak SEP intensity with the CME speed less sensitive to the connection distance than the correlation with the SXR peak flux.

At the present time such interpretation is speculative. Irrespective of the physical relationships, the usefulness of either the CME speed or the SXR peak flux in empirical schemes of SEP prediction is confirmed by the present study, with a greater sensitivity to the angular connection if the peak SXR flux is used.

Appendix

Tables 4 – 6 summarize all data used in the paper, organized in different IMF categories, namely ICME, SoWi and SEP events in the vicinity of an ICME (Section 3.1). The events in each table are listed chronologically: The event date is given in column (1). The proton and electron peak intensities (with their onset time) follow in columns (2) – (5). The next four columns give the SXR peak flux (with the onset time), the flare position on the western (W) hemisphere, the projected CME speed and the angular width (AW), as reported in catalogs or from previous work. The data sources are explained in detail in the footnotes under each table. In column (10) we give the temporal offset between the GOES SEP start (or at *Wind* at 1 AU) and the nearest-in-time boundary of the ICME (shifted at GOES orbit or as observed at 1 AU). This value is used as a confidence check for the identification of the IMF category. Although we used exclusively the timings of the ICME boundaries as reported in Richardson and Cane (2010), differences might exist with other ICME lists due to different definition used for an ICME, variation in the IMF data from different satellites and also due to the subjectivity of the observer. In the ICME category (Table 4) two events are relatively close (about 2 h) to the reported ICME onset and may change category after a detailed analysis. All other events in this category are well within the body of the ICME. Similarly for the last SEP category (Table 6), some SEP events might be propagating in quiet solar wind conditions, although many are in the sheath region of the ICME or occur only several hours before or after the ICME boundary. Rise times are given in column (11) in Tables 4 and 5. Finally, in the last two columns in each table the solar wind speed (averaged values) and the connection distance are given.

The linear regression between the $\log I_{SXR} - \log V_{CME}$ is given in Table 11 and the dependencies between $\log J_{max}$ and the logarithms of the parameters of coronal activity are summarized in Table 12.

Table 4 ICME solar energetic particle events.

Event date yy mm dd	Particle intensity (cm^2 s MeV sr)$^{-1}$		ACE/EPAM ($\times 10^4$)		Flare		CME		SEP		SoWi speed [km s^{-1}]	Conn. dist. [deg]
	GOES 15–40 [MeV]	Wind/EPACT 19–28 [MeV]	38–53 [keV]	175–135 [keV]	Peak SXR flux [W m^{-2}]	Long. W [deg]	speed [km s^{-1}]	AW [deg]	offset [h]	Rise time (2)/(3)/(4)/(5) [min]		
(1)	(2)	(3)	(4)	(5)	(6)	(7)	(8)	(9)	(10)	(11)	(12)	(13)
98 05 02	5.2 (14:00)	1.5 (14:00)	22 (13:55)	1	X1.1 (13:31)	15	938	130	− 8.2	8/18/19/5	619	− 23
98 05 06	8.7 (08:30)	5.7 (08:30)	140 (08:10)	4.1	X2.7 (07:58)	65	1099	90	+ 39.2	9/11/4/–	506	18
99 12 28	–	0.006^w (02:00)	3.6 (01:45)	0.11	M4.5 (00:39)	56	672	60	+ 2	–/–/62/18	465	5
00 06 25	0.04 (12:30)^d	0.03 (12:00)^d	0.45 (08:00)	0.0032	M1.9 (07:17)	55	1617	70	+ 20.3	u	508	9
00 07 14	312 (10:30)	88 (10:40)	72 (10:40)	12	X5.7 (10:03)	7	1674	360	+ 5.2	11/6/5/6	579	− 34
00 08 12	0.06 (11:00)	0.05^u (11:00)	0.47 (10:55)	0.0046	M1.1 (09:45)	(79)	662	60	− 5.3	u	617	(41)
00 09 09	–	0.02 (10:00)	0.21 (10:00)	0.0077	M1.6 (08:28)	67	554	70	− 22	–/–/25/58	468	17
00 09 19	0.03 (14:00)^d	0.02 (13:00)^d	2.3 (09:15)	0.019	M5.1 (08:06)	46	766	60	+ 34.7	u/u/81/65	672	11
00 11 08	377 (23:30)	179^u (23:00)	240 (23:00)	32	M7.4 (22:42)	[78]	1738	120	− 9.6	6/4/4/2	460	[27]
01 03 29	0.9 (12:30)	0.66 (12:00)	7.9 (10:37)	0.35	X1.7 (09:57)	19	942	360	− 18.7	69/45/74/20	566	− 23
01 04 02	0.09 (12:00)	0.08 (13:00)	–	–	X1.1 (10:58)	(62)	992	50	+ 28.8	119/6^u/–/–	585	(22)
01 04 02	43 (23:00)	36^m (23:00)	46 (22:05)	2.2	X20 (21:32)	[70]	2505	100	+ 16.7	18/4/14/9	543	[27]
01 04 12	1^m (11:30)	0.75^m (12:00)	–	–	X2.0 (09:39)	43	1184	120	− 12.9	u/–	633	6
01 10 22	0.5 (16:40)^d	0.4 (17:00)^d	0.92 (01:13)	0.0076	M1.0 (00:22)	57	772	20	− 8	53/u/186/196	553	14
02 04 21	81.5 (01:30)	81 (01:30)	84 (01:40)	3.5	X1.5 (00:43)	84	2393	120	+ 17.3	15/11/3/2	485	35
02 08 03	–	0.007^w (00:00)nd	0.9 (20:05)	0.01	X1.0 (18:59)	76	1150	30	+ 2.4	–/u	497	29
02 08 20	0.07 (09:00)	0.37 (09:00)	40 (08:52)	1.3	M3.4 (08:22)	38	1099	40	− 20.1	54/37/14/13	466	− 13
02 12 22	–	0.02^w (14:00)^d	–	–	M1.1 (02:14)	42	1071	80	+ 5	–	454	− 10
03 05 31	0.73 (03:00)	0.57 (03:00)	14 (02:55)	0.65	M9.3 (02:13)	65	1835	150	− 4.4	20/15/19/9	702	31

Table 4 (*Continued.*)

Event date yy mm dd	Particle intensity $(cm^2\,s\,MeV\,sr)^{-1}$				Flare		CME		SEP		SoWi	Conn.
	GOES $15-40$ [MeV]	*Wind*/EPACT $19-28$ [MeV]	ACE/EPAM $(\times 10^4)$ $38-53$ [keV]	$175-135$ [keV]	Peak SXR flux $[W\,m^{-2}]$	Long. W [deg]	speed $[km\,s^{-1}]$	AW [deg]	offset [h]	Rise time (2)/(3)/(4)/(5) [min]	speed $[km\,s^{-1}]$	dist. [deg]
(1)	(2)	(3)	(4)	(5)	(6)	(7)	(8)	(9)	(10)	(11)	(12)	(13)
03 08 19	–	0.007 (10:00)	2.9^w (08:30)	0.045	M2.0 (07:38)	63	412	40	+ 5.9	–/–/16/15	467	12
03 10 29	57^m (21:30)	94^m (21:30)	150 (22:05)	12	X10 (20:37)	2	2029	360	+ 5.8	u	812^s	− 27
04 11 10	1.5^m (03:00)	5.5^m (06:00)	–	–	X2.5 (01:59)	49	3387	120	− 6.4	14/37/–/–	758	18

Column (7) lists the heliographic west longitude of the flare according to: the preliminary listings of the GOES solar X-ray flares in the *Solar Geophysical Data* (SGD), the corresponding Hα flare longitude in the comprehensive reports in the SGD (in the parentheses), or the daily flare active region longitude reported in SolarMonitor.org (in square brackets). In column (9), the angular width (Cane, Richardson, and von Rosenvinge, 2010) of the corresponding CME is given. Column (10) lists the temporal offset in hours between the SEP start at GOES data (or *Wind*/EPACT when no event in GOES is observed) and the nearest ICME boundary, *i.e.*, a positive value denotes the time from the SEP onset to the end of the ICME and a negative value – to the start of the ICME.

d: delayed SEP onset; m: multiple SEP intensity peaks; nd: next day; s: strong increase in the solar wind speed (1-h average data) during the 6-h period before the SEP onset; w: weak SEP intensity; u: uncertain.

Table 5 SoWi solar energetic particle events.

Event date yy mm dd	Particle intensity (cm^2 s MeV sr)$^{-1}$				Flare		CME		AW [deg]	SEP		SoWi speed [km s^{-1}]	Conn. dist. [deg]
	GOES 15–40 [MeV]	Wind/EPACT 19–28 [MeV]	ACE/EPAM (×10^4) 38–53 [keV]	175–135 [keV]	Peak SXR flux [W m^{-2}]	Long. W [deg]	speed [km s^{-1}]			offset [days]	Rise time (2)/(3)/(4)/(5) [min]		
(1)	(2)	(3)	(4)	(5)	(6)	(7)	(8)	(9)		(10)	(11)	(12)	(13)
97 05 21	–	0.006^w (21:00)	–	–	M1.3 (20:08)	12	296	30		+4.8	–	311	−64
97 11 03	–	0.005^u (12:00)	0.23 (10:50)	0.0059	M4.2 (10:18)	(22)	352	100		+3.7	–	317	(−52)
97 11 04	2^m (06:30)	1 (07:00)	12 (06:24)	0.46	X2.1 (05:52)	33	785	110		+2.9	22/38/–/–	307	−44
98 11 05	0.0006 (<22:00)	Cane, Richardson, and von Rosenvinge (2010)	–	–	M8.4 (19:00)	18	1118	60		+2	–	433	−36
98 12 17	0.0003 (11:00)	Cane, Richardson, and von Rosenvinge (2010)	0.4 (08:20)	0.0086	M3.2 (07:40)	46	302	–		+12.3	–/–/13/60	382	−16
99 08 28	0.0005 (20:00)	Cane, Richardson, and von Rosenvinge (2010)	–	–	X1.1 (17:52)	14	462	110		−5.4	–	642	−23
00 03 03	–	0.01^w (03:00)	1 (02:30)	0.029	M3.8 (02:08)	60	841	80		−1	–/u/24/<5	423	4
00 03 22	0.03 (19:00)	0.02 (19:00)	–	–	X1.1 (18:34)	57	478	80		−3.25	u/–	473	7
00 04 04	0.62 (16:30)	0.57 (18:00)	17.5 (15:33)	0.0946	C9.7 (15:12)	66	1188	60		+2.7	29/53/4/<5	380	4
00 05 01	0.04 (10:30)	0.007^u (11:00)	74 (10:23)	1.3	M1.1 (10:16)	54^c	1360	20		+1.4	u/u/<5/<5	436	0
00 06 15	0.001 (21:00)	Cane, Richardson, and von Rosenvinge (2010)	7.3 (19:52)	0.025	M1.8 (19:38)	65	1081	70		−1.6	–/–/<5/<5	606	26
00 06 17	0.03 (05:00)	0.01 (05:00)	16 (03:20)	0.086	M3.5 (02:25)	72	857	60		+1.2	u/u/12/20	472	22
00 07 22	0.52 (12:00)	0.34^m (12:00)	–	–	M3.7 (11:17)	56	1230	80		+1.1	22/32/–/–	449	3
00 09 12	5.5 (14:30)	3.4 (14:00)	4.5 (12:47)	0.26	M1.0 (11:31)	9	1550	100		−2.1	36/53/13/14	468	−41
00 11 24	0.23 (06:30)	0.15 (06:00)	2.3 (05:50)	0.078	X2.0 (04:55)	(5)	1289	360		+3.1	45/80/63/59	318	(−69)
00 11 24	2.2^m (15:30)	1.8^m (15:30)	14 (15:43)	0.51	X2.3 (14:51)	7	1245	360		+2.7	64/79/28/29	410	−50
01 01 28	0.73 (16:30)	0.63^m (16:30)	5.1 (16:35)	0.2	M1.5 (15:40)	59	916	120		−2.4	24/68/30/15	326	−13
01 03 10	0.002 (08:00)	Cane, Richardson, and von Rosenvinge (2010)	0.73 (05:40)	0.028	M6.7 (04:00)	42	819	20		−5.3	–/–/33/57	419	−14
01 04 10	2.7 (08:00)	2.6 (08:00)	5.8 (05:55)	0.21	X2.3 (05:06)	9	2411	360		−1.1	76/123/162/130	535	−35

Table 5 (*Continued.*)

Event date yy mm dd	Particle intensity (cm^2 s MeV sr)$^{-1}$ GOES 15–40 [MeV]	Wind/EPACT 19–28 [MeV]	ACE/EPAM (×10^4) 38–53 [keV]	175–135 [keV]	Flare Peak SXR flux [W m^{-2}]	Long. W [deg]	CME speed [km s^{-1}]	AW [deg]	SEP offset [days]	Rise time (2)/(3)/(4)/(5) [min]	SoWi speed [km s^{-1}]	Conn. dist. [deg]
(1)	(2)	(3)	(4)	(5)	(6)	(7)	(8)	(9)	(10)	(11)	(12)	(13)
01 04 26	0.0003 (<22:00)	Cane, Richardson, and von Rosenvinge (2010)	0.7 (13:30)	0.0051	M7.8 (11:26)	31	1006	360	+1.7	–/–/19/w	433	– 25
01 07 19	0.0003 (11:00)	Cane, Richardson, and von Rosenvinge (2010)	0.88 (10:20)	0.018	M1.8 (09:52)	62	1668	40	– 5.4	–/–70^u/77	601	23
01 10 19	0.18 (02:00)	0.14 (02:30)	1.1 (02:20)	0.036	X1.6 (00:47)	18	558	180	+2.8	34/81/32/51	309	– 58
01 10 19	0.18 (17:30)	0.22^m (17:30)	1.9 (17:10)	0.039	X1.6 (16:13)	29	901	160	+2.1	81/139/27/35	326	– 43
01 11 04	39^m (16:30)	284 (16:30)	88 (16:45)	5.7	X1.0 (16:03)	18	1810	130	+1.1	101/19/8/4	310	– 58
01 11 22	177 (21:00)	103 (21:00)	64 (21:00)	3.1	M3.8 (20:18)	67	1443	120	– 1.3	16/35/19/7	433	13
01 12 26	23 (05:30)	22 (06:00)	80 (05:40)	2.5	M7.1 (04:32)	54	1446	90	+1.8	11/16/6/6	384	– 7
02 02 20	0.55 (06:30)	0.24 (06:30)	43 (06:05)	0.9	M5.1 (05:52)	72	952	50	+8.5	13/6/3/5	404	14
02 03 15	0.05 (02:00)nd	0.01^u (01:00)nd	0.9 (00:30)nd	0.027	M2.2 (22:09)	3	957	360	+3.2	350/485/39/35	345	– 65
02 04 15	...(03:00)	Cane, Richardson, and von Rosenvinge (2010)	4.8 (03:00)	0.029	C9.8 (02:46)	79	674	45	– 1.6	–/–/<5/<5	373	16
02 07 15	1.3 (11:00)nd	1^m (09:00)nd	–	–	X3.0 (19:59)	1	1151	100	+2.1	91/120/–/–	344	– 68
02 08 14	0.29^m (02:30)	0.32^m (02:30)	78 (02:00)	0.48	M2.3 (01:47)	54	1309	60	+5.45	u/u/3/6	444	1
02 08 16	0.02 (07:00)	0.01^w (08:00)	19 (06:30)	0.054	M2.4 (05:46)	83	1378	70	+3.3	u/u/3/5	597	44
02 08 24	10^m (01:30)	10^m (01:30)	19 (01:30)	1.1	X3.1 (00:49)	81	1913	150	– 2.4	13/7/5/5	384	20
02 11 09	9.2 (15:00)	8.3 (15:30)	1.9 (14:00)	0.055	M4.6 (13:08)	29	1838	90	+7.8	31/31/23/26	365	– 36
03 03 17	0.02 (20:00)	0.01 (19:30)	2.9 (19:14)	0.052	X1.5 (18:50)	39	1020	50	– 1.9	u/u/8/<5	722	6
03 03 18	0.03 (14:00)	0.01 (14:00)	49 (12:30)	0.32	X1.5 (11:51)	46	1042	80	– 1.1	u/u/5/8	762	15
03 04 23	w	0.01 (02:00)	0.15 (01:15)	0.0076	M5.1 (00:39)	25	916	70	+16.2	u/u/u/15	518	– 21
03 04 24	0.04 (13:30)	0.02 (13:00)	0.91 (13:10)	0.0093	M3.3 (12:45)	39	609	45	+14.75	60/u/8/<5	459	– 12
03 05 27	0.0003 (22:00)	Cane, Richardson, and von Rosenvinge (2010)	–	–	X1.3 (22:56)	17	964	360	+1.6	–	468	– 30

Table 5 (*Continued.*)

Event date yy mm dd	Particle intensity (cm² s MeV sr)⁻¹				Flare		CME		SEP		SoWi speed [km s⁻¹]	Conn. dist. [deg]
	GOES 15–40 [MeV]	Wind/EPACT 19–28 [MeV]	ACE/EPAM (×10⁴)		Peak SXR flux [W m⁻²]	Long. W [deg]	speed [km s⁻¹]	AW [deg]	offset [days]	Rise time (2)/(3)/(4)/(5) [min]		
			38–53 [keV]	175–135 [keV]								
(1)	(2)	(3)	(4)	(5)	(6)	(7)	(8)	(9)	(10)	(11)	(12)	(13)
03 11 04	11.7 (21:30)	10.5 (21:25)	6 (20:25)	0.38	X28 (19:29)	83	2657	130	− 2.9	123/100/u/187	637	46
04 02 04	–	0.006ʷ (12:00)	0.5 (11:26)	0.0097	C9.9 (11:12)	48	764	20	− 10.3	–/–243/42	568	6
04 04 11	0.64 (06:00)	0.5 (06:00)	2.9 (04:36)	0.14	C9.6 (03:54)	47	1645	90	− 5.5	39/37/<5/10	441	− 6
04 07 13	0.04 (01:00)	0.03 (01:30)	0.17 (00:40)	0.0063	M6.7 (00:09)	(60)	607	60	+ 9.7	71/327/122/74	506	[13]
04 10 30	0.06 (07:00)	0.03ᵐ (07:30)	5.4ᵘ (06:25)	0.062ᵘ	M4.2 (06:08)	21	422	90	+ 8.65	110/251/114/21	387	− 40
05 05 06	0.05 (07:30)	0.03 (05:00)	8.4 (03:47)	0.078	C9.3 (03:05)	(74)	1120	20	+ 9	380/202/52/62	338ˢ	(4)
05 05 06	0.03 (16:30)	0.03 (15:00)	30 (12:00)	0.046	M1.3 (11:11)	(80)	1144	30	+ 8.5	u/u/86/82	357	(14)
05 05 11	0.03ⁿᵈ (21:30)	0.01 (21:00)	0.8 (20:00)	0.0074	M1.1 (19:22)	(47)	550	70	+ 3.4	u/u/38/79	461	(− 4)
05 07 13	0.0003 (05:00)	Cane, Richardson, and von Rosenvinge (2010)	4.7 (04:10)	0.013	M1.1 (02:35)	[79]	759	40	− 1.04	–/–16/30	525	[34]
05 07 13	0.34 (16:30)	0.22 (16:00)	23 (14:40)	0.22	M5.0 (14:01)	(80)	1423	70	− 1.5	133/168/26/16	580	(39)
05 08 22	0.22 (02:00)	0.2 (02:00)	11 (01:17)	0.15	M2.6 (00:44)	(48)	1194	160	+ 1.95	47/42/5/13	537	(4)
05 08 22	10.7 (19:00)	8.5 (19:00)	58 (17:40)	1.2	M5.6 (16:46)	(62)	2378	100	+ 1.25	47/66/16/15	545	[19]
06 07 06	0.08 (09:00)	0.07 (10:00)	0.24 (09:05)	0.0057	M2.5 (08:13)	(32)	911	160	+ 4.5	65/22/23ᵘ/69ᵘ	576	(− 9)
06 12 13	25 (02:30)	20.4 (03:00)	120 (02:41)	5.4	X3.4 (02:14)	(24)	1774	180	+ 1.8	17/23/<5/<5	665ᵂ	(− 13)

Here, column (10) lists the temporal offset in days between the SEP start from GOES data (or *Wind*/EPACT when no event in GOES is observed) and the nearest ICME boundary: Positive (negative) values denote the time from the SEP onset to the start (end) of the ICME following (preceding) the SEP event, respectively.

c: flare longitude as reported by Cane, Richardson, and von Rosenvinge (2010); d: delayed SEP onset; m: multiple SEP intensity peaks; nd: next day; s: strong increase in the solar wind speed (1-h average data) during the 6-h period before the SEP onset; w: weak SEP intensity; W: solar wind data from *Wind*/SWE; u: uncertain.

Table 6 Solar energetic particle events in the vicinity of an ICME.

Event date yy mm dd	Particle intensity (cm² s MeV sr)⁻¹		ACE/EPAM		Flare	Long. W [deg]	CME speed [km s⁻¹]	AW [deg]	SEP offset [h]	SoWi speed [km s⁻¹]	Conn. dist. [deg]
	GOES 15–40 [MeV]	Wind/EPACT 19–28 [MeV]	38–53 [keV]	175–135 [keV]	Peak SXR flux [W m⁻²]						
(1)	(2)	(3)	(4)	(5)	(6)	(7)	(8)	(9)	(10)	(11)	(12)
97 11 06	14.6 (12:30)	13.2 (12:30)	47 (12:35)	3.4	X9.4 (11:49)	63	1556	115	+16.5	359	−3
99 06 04	1.4 (08:15)	1^m (08:00)	16 (07:22)	0.53	M3.9 (06:52)	69	2230	80	−9.3	428	14
99 06 27	–	0.01 (10:00)	1.1 (09:00)	0.0164	M1.0 (08:34)	25	903	40	+10	479	−24
00 02 12	0.05 (05:20)	0.05 (06:00)	1.1 (04:50)	0.013	M1.7 (03:51)	23	1107	110	sheath	573	−18
00 03 02	0.03 (09:00)	0.02 (10:00)	0.51 (08:46)	0.025	X1.1 (08:20)	(52)	776	60	−5.15	437	(−2)
00 05 23	0.002 (22:00)	Cane, Richardson, and von Rosenvinge (2010)	4.7 (–)	0.031	C9.5 (20:48)	43	475	50	sheath	591	3
00 06 10	1.4 (17:30)	1.7 (17:30)	60 (17:09)	0.53	M5.2 (16:40)	38	1108	120	−0.01	512	−8
00 06 18	0.07 (02:30)	0.05^m (03:00)	3.2 (02:22)	0.067	X1.0 (01:52)	85	629	70	+7.6	432	−30
00 06 23	0.05 (15:45)	0.02 (15:30)	23 (14:45)	0.16	M3.0 (14:18)	72	847	60	sheath	494	24
01 04 09	0.16 (16:35)	0.1 (17:00)	1.7 (16:34)	0.081	M7.9 (15:20)	4	1194	360	−12.6	521	−41
01 04 14	–	0.02^u (18:00)	51 (17:35)	0.43	M1.0 (17:15)	71	830	50	−6	655	35
01 04 15	30.4 (14:00)	30.5 (14:00)	62 (14:05)	5.5	X14.4 (13:19)	85	1129	110	+2.8	499	38
01 09 12	–	0.01^u (22:30)	–	–	C9.6 (21:05)	62^c	668	30	+19.5	356	−4
01 09 15	0.33 (12:10)	0.19 (12:30)	2.3 (12:07)	0.028	M1.5 (11:04)	49	478	80	−13.2	526	4
02 04 11	0.03 (17:30)	0.08 (17:00)	6.1 (16:40)	0.0155	C9.2 (16:16)	33	540	50	+8	475	−17
02 04 14	–	0.01 (13:00)^d	0.8 (09:00)	–	C9.6 (07:28)	57	757	50	−23.9	386	−4
02 04 17	0.47 (11:20)^d	0.46 (11:00)^d	84 (–)	0.67	M2.6 (07:46)	34	1240	70	+5.5	333	−37
02 08 18	0.05 (22:35)	0.06 (23:00)	12 (21:41)	0.11	M2.2 (21:12)	19	682	100	sheath	472^s	−31

Table 6 (*Continued.*)

Event date yy mm dd	Particle intensity (cm² s MeV sr)⁻¹		ACE/EPAM (×10⁴)		Flare		CME		SEP offset [h]	SoWi speed [km s⁻¹]	Conn. dist. [deg]
	GOES 15–40 [MeV]	Wind/EPACT 19–28 [MeV]	38–53 [keV]	175–135 [keV]	Peak SXR flux [W m⁻²]	Long. W [deg]	speed [km s⁻¹]	AW [deg]			
(1)	(2)	(3)	(4)	(5)	(6)	(7)	(8)	(9)	(10)	(11)	(12)
02 08 19	*0.017 (10:00)*	Cane, Richardson, and von Rosenvinge (2010)	55 (10:55)	0.47	M2.0 (10:28)	25	549	80	sheath	532	−19
02 08 22	1.1 (02:50)	0.5^m (03:00)	10 (02:21)	0.15	M5.4 (01:47)	62	998	80	−12.1	416	5
02 12 19	0.06 (00:55)nd	0.11 (22:30)	6.6 (22:00)	0.16	M2.7 (21:34)	(9)	1092	120	−12	478	(−40)
03 10 26	14.5^m (18:00)	9.4^m (18:00)	34 (17:53)	0.16	X1.2 (17:21)	38	1537	130	+4.9	468	−10
03 11 02	60 (17:30)	52.6 (18:00)	40 (17:42)	4.1	X8.3 (17:03)	56	2598	130	−17	533	−12
03 11 20	0.14 (08:40)	0.08 (08:00)	14.2 (08:18)	0.266	M9.6 (07:35)	8	669	90	sheath	503^s	−39
04 07 25	1.6 (16:30)	1.4^m (16:00)	13 (15:27)	0.35	M1.1 (14:19)	33	1333	130	sheath	590	−7
04 11 07	14.2^m (17:30)	11.8^m (18:00)	17 (17:00)	0.08	X2.0 (15:42)	17^c	1759	150	+3.15	436	−37
04 11 09	1.7 (19:40)	1.1^m (19:30)	46 (18:05)	0.46	M8.9 (16:59)	51	2000	130	sheath	690	17
05 01 15	11.2 (00:00)nd	0.2 (07:00)nd	92 (23:15)	1.3	X2.6 (22:25)	(3)	2861	130	+14.8	567^W	(−37)
05 01 17	181^m (13:30)^d	205^m (13:00)^d	280 (10:00)	19	X3.8 (06:59)	(24)	2094	110	−5.7	577	(−16)
05 01 20	53 (07:00)	66.3 (07:00)	110 (06:46)	12	X7.1 (06:36)	58	882	80	−3.5	822^s	32
05 07 09	0.08 (02:30)nd	0.1^m (01:00)nd	2.3 (23:15)	0.038	M2.8 (21:47)	(27)	1540	65	+8.5	345	(−41)
05 07 12	–	0.007^u (18:00)	1.2 (17:13)	0.012	M1.5 (15:47)	(64)	523	80	−14	502	(17)
06 12 14	8.1 (22:30)	0.6^m (00:40)nd	6 (22:50)	0.23	X1.5 (21:07)	(46)	1042	70	−0.05	936	(21)

In column (10) positive (negative) values denote the time in hours from the SEP (GOES) onset to the start (end) of the following (preceding) ICME, respectively.

c: flare longitude as reported by Cane, Richardson, and von Rosenvinge (2010); d: delayed SEP onset; m: multiple SEP intensity peaks; nd: next day; s: strong increase in the solar wind speed (1-h average data) during the 6-h period before the SEP onset; w: weak SEP intensity; W: solar wind data from *Wind*/SWE; u: uncertain.

Table 7 Linear correlation coefficients (with standard deviations) between $\log J_{max}$ and $\log I_{SXR}$ or $\log V_{CME}$ for GOES proton and ACE/EPAM low energy electron data, for the entire event sample (*i.e.* no event restriction) and for different sub-samples. The number of events in each group is given in brackets.

SEP event sub-samples	IMF categories of SEP events		
	ICME	SoWi	All SEPs
Protons	GOES 15 – 40 MeV		
$\log J_p$–$\log V_{CME}$			
No event restriction	0.57 ± 0.15 (17)	0.66 ± 0.07 (38)	0.63 ± 0.05 (81)
Flares > W30°	0.59 ± 0.16 (13)	0.61 ± 0.11 (26)	0.59 ± 0.08 (56)
Flares > W50°	0.63 ± 0.20 (9)	0.60 ± 0.12 (17)	0.58 ± 0.11 (36)
Flares > W60°	0.76 ± 0.22 (7)	0.65 ± 0.14 (11)	0.64 ± 0.09 (24)
$\log J_p$–$\log I_{SXR}$			
No event restriction	0.67 ± 0.13 (17)	0.36 ± 0.13 (38)	0.59 ± 0.07 (81)
Flares > W30°	0.58 ± 0.16 (13)	0.36 ± 0.18 (26)	0.56 ± 0.09 (56)
Flares > W50°	0.61 ± 0.17 (9)	0.52 ± 0.14 (17)	0.62 ± 0.09 (36)
Flares > W60°	0.51 ± 0.34 (7)	0.54 ± 0.17 (11)	0.60 ± 0.11 (24)
Electrons	ACE/EPAM 38 – 53 keV		
$\log J_e$–$\log V_{CME}$			
No event restriction	0.64 ± 0.14 (18)	0.55 ± 0.09 (46)	0.53 ± 0.07 (96)
Flares > W30°	0.60 ± 0.16 (14)	0.57 ± 0.11 (33)	0.56 ± 0.07 (68)
Flares > W50°	0.62 ± 0.17 (11)	0.45 ± 0.22 (21)	0.53 ± 0.10 (45)
Flares > W60°	0.72 ± 0.16 (9)	0.14 ± 0.28 (15)	0.52 ± 0.13 (32)
$\log J_e$–$\log I_{SXR}$			
No event restriction	0.73 ± 0.10 (18)	0.12 ± 0.11 (46)	0.40 ± 0.08 (84)
Flares > W30°	0.67 ± 0.12 (14)	0.08 ± 0.12 (33)	0.35 ± 0.08 (68)
Flares > W50°	0.72 ± 0.12 (11)	-0.02 ± 0.17 (21)	0.35 ± 0.11 (45)
Flares > W60°	0.67 ± 0.18 (9)	0.11 ± 0.28 (15)	0.38 ± 0.13 (32)

Table 8 Correlation coefficients with standard deviations of the particle fluence, Φ, with the flare and CME parameters.

Correlation $\log \Phi$ with:	IMF categories of SEP events	
	ICME	SoWi
Protons	GOES/*Wind*-EPACT	
$\log I_{SXR}$	$0.62 \pm 0.13/0.71 \pm 0.09$	$0.34 \pm 0.15/0.38 \pm 0.11$
$\log V_{CME}$	$0.53 \pm 0.17/0.73 \pm 0.08$	$0.66 \pm 0.08/0.63 \pm 0.06$
AW	$0.59 \pm 0.14/0.63 \pm 0.11$	$0.23 \pm 0.14/0.34 \pm 0.14$
Number	17/22	35/43
Electrons	ACE-EPAM low/high energy channel	
$\log I_{SXR}$	$0.63 \pm 0.18/0.77 \pm 0.09$	$0.18 \pm 0.11/0.37 \pm 0.11$
$\log V_{CME}$	$0.68 \pm 0.15/0.82 \pm 0.07$	$0.63 \pm 0.07/0.72 \pm 0.05$
AW	$0.41 \pm 0.13/0.61 \pm 0.11$	$0.03 \pm 0.16/0.17 \pm 0.17$
Number	16	42

Table 9 Linear correlation coefficients (with standard deviations) between $\log \Phi_{p,e}$ and $\log I_{SXR}$ or $\log V_{CME}$ for GOES proton and ACE/EPAM low energy electron data, for the entire event sample (*i.e.* no event restriction) and for different sub-samples. The number of events in each group is given in brackets.

SEP event sub-samples	IMF categories of SEP events	
	ICME	SoWi
Protons	GOES 15 – 40 MeV	
$\log \Phi_p$–$\log V_{CME}$		
No event restriction	0.53 ± 0.17 (17)	0.66 ± 0.08 (35)
Flares > W30°	0.58 ± 0.17 (13)	0.59 ± 0.12 (23)
Flares > W50°	0.69 ± 0.17 (6)	0.60 ± 0.12 (16)
Flares > W60°	0.82 ± 0.20 (7)	0.69 ± 0.20 (9)
$\log \Phi_p$–$\log I_{SXR}$		
No event restriction	0.62 ± 0.13 (17)	0.34 ± 0.15 (35)
Flares > W30°	0.52 ± 0.17 (13)	0.35 ± 0.17 (23)
Flares > W50°	0.55 ± 0.20 (9)	0.41 ± 0.18 (16)
Flares > W60°	0.47 ± 0.38 (7)	0.41 ± 0.23 (9)
Electrons	ACE/EPAM 38 – 53 keV	
$\log \Phi_e$–$\log V_{CME}$		
No event restriction	0.68 ± 0.15 (16)	0.63 ± 0.07 (42)
Flares > W30°	0.66 ± 0.17 (12)	0.65 ± 0.08 (31)
Flares > W50°	0.66 ± 0.19 (10)	0.59 ± 0.15 (21)
Flares > W60°	0.64 ± 0.22 (9)	0.41 ± 0.21 (15)
$\log \Phi_e$–$\log I_{SXR}$		
No event restriction	0.63 ± 0.18 (16)	0.18 ± 0.11 (42)
Flares > W30°	0.60 ± 0.21 (12)	0.07 ± 0.12 (31)
Flares > W50°	0.60 ± 0.23 (10)	0.10 ± 0.15 (21)
Flares > W60°	0.57 ± 0.26 (9)	0.20 ± 0.23 (15)

Table 10 Correlation coefficients with standard deviations of the J_{max} with the flare and CME parameters with respect to the connection distance of the particles for the *Wind*/EPACT proton and ACE/EPAM low energy channel electron data.

Correlation $\log J_{max}$ with:	IMF categories of SEP events	
	ICME	SoWi
Protons	Inner events/Outer events/All events in category	
$\log I_{SXR}$	$0.70 \pm 0.24 / 0.59 \pm 0.18 / 0.71 \pm 0.10$	$0.41 \pm 0.20 / 0.42 \pm 0.18 / 0.41 \pm 0.11$
$\log V_{CME}$	$0.67 \pm 0.21 / 0.75 \pm 0.11 / 0.73 \pm 0.09$	$0.68 \pm 0.10 / 0.71 \pm 0.08 / 0.69 \pm 0.06$
Electrons	Inner events/Outer events/All events in category	
$\log I_{SXR}$	$0.78 \pm 0.13 / 0.62 \pm 0.33 / 0.73 \pm 0.10$	$0.15 \pm 0.21 / 0.14 \pm 0.11 / 0.12 \pm 0.11$
$\log V_{CME}$	$0.29 \pm 0.37 / 0.83 \pm 0.33 / 0.40 \pm 0.08$	$0.74 \pm 0.07 / 0.41 \pm 0.16 / 0.55 \pm 0.09$

Table 11 Relationship between $\log I_{SXR}$ and $\log V_{CME}$ for flare/CME events associated with GOES proton and ACE/EPAM electron SEP events, derived from the linear fits.

	IMF category	$\log V_{CME} = a + b \log I_{SXR}$		$\log I_{SXR} = c + d \log V_{CME}$	
		a	b	c	d
Protons	ICME	-5.87	1.90	3.11	0.20
	SoWi	-2.27	0.66	3.08	0.08
	All SEPs	-3.81	1.20	3.09	0.13
Electrons	ICME	-6.24	2.02	3.07	0.24
	SoWi	-2.57	0.74	3.06	0.11
	All SEPs	-4.26	1.32	3.07	0.16

Table 12 Relationship between $\log J_{max}$ and the flare and CME parameters for the GOES proton and ACE/EPAM electron SEP events, derived from the linear fits.

	IMF category	$\log J_{max} = a + b \log I_{SXR}$		$\log J_{max} = c + d \log V_{CME}$	
		a	b	c	d
Protons	ICME	0.23	1.45	-11.6	3.80
	SoWi	-0.15	0.70	-11.8	3.74
	All SEPs	0.07	1.17	-11.7	3.77
Electrons	ICME	5.04	1.10	-3.48	2.76
	SoWi	4.76	0.18	-1.87	2.18
	All SEPs	5.01	0.55	-1.46	2.09

References

Bai, T.: 1987, Distribution of flares on the Sun – superactive regions and active zones of 1980 – 1985. *Astrophys. J.* **314**, 795 – 807. doi:10.1086/165105.

Bein, B.M., Berkebile-Stoiser, S., Veronig, A.M., Temmer, M., Vrsnak, B.: 2012, Impulsive acceleration of coronal mass ejections: II. Relation to SXR flares and filament eruptions. ArXiv e-prints.

Burkepile, J.T., Hundhausen, A.J., Stanger, A.L., St. Cyr, O.C., Seiden, J.A.: 2004, Role of projection effects on solar coronal mass ejection properties: 1. A study of CMEs associated with limb activity. *J. Geophys. Res.* **109**, A03103. doi:10.1029/2003JA010149.

Cane, H.V., Richardson, I.G., von Rosenvinge, T.T.: 2010, A study of solar energetic particle events of 1997 – 2006: their composition and associations. *J. Geophys. Res.* **115**, A08101. doi:10.1029/2009JA014848.

Chertok, I.M.: 1990, On the correlation between the solar gamma-ray line emission, radio bursts and proton fluxes in the interplanetary space. *Astron. Nachr.* **311**, 379 – 381.

Cliver, E.W., Forrest, D.J., Cane, H.V., Reames, D.V., McGuire, R.E., von Rosenvinge, T.T., Kane, S.R., MacDowall, R.J.: 1989, Solar flare nuclear gamma-rays and interplanetary proton events. *Astrophys. J.* **343**, 953 – 970. doi:10.1086/167765.

Garcia, H.A.: 2004, Forecasting methods for occurrence and magnitude of proton storms with solar hard X rays. *Space Weather* **2**, S06003. doi:10.1029/2003SW000035.

Gold, R.E., Krimigis, S.M., Hawkins, S.E. III, Haggerty, D.K., Lohr, D.A., Fiore, E., Armstrong, T.P., Holland, G., Lanzerotti, L.J.: 1998, Electron, proton, and alpha monitor on the advanced composition explorer spacecraft. *Space Sci. Rev.* **86**, 541 – 562. doi:10.1023/A:1005088115759.

Gopalswamy, N., Yashiro, S., Lara, A., Kaiser, M.L., Thompson, B.J., Gallagher, P.T., Howard, R.A.: 2003, Large solar energetic particle events of cycle 23: a global view. *Geophys. Res. Lett.* **30**(12), SEP3-1. doi:10.1029/2002GL016435.

Gopalswamy, N., Yashiro, S., Krucker, S., Stenborg, G., Howard, R.A.: 2004, Intensity variation of large solar energetic particle events associated with coronal mass ejections. *J. Geophys. Res.* **109**, A12105. doi:10.1029/2004JA010602.

Hovestadt, D., Hilchenbach, M., Bürgi, A., Klecker, B., Laeverenz, P., Scholer, M.: 1995, CELIAS – Charge, Element and Isotope Analysis System for SOHO. *Solar Phys.* **162**, 441–481. doi:10.1007/BF00733436.

Kahler, S.W.: 1982a, Radio burst characteristics of solar proton flares. *Astrophys. J.* **261**, 710–719. doi:10.1086/160381.

Kahler, S.W.: 1982b, The role of the big flare syndrome in correlations of solar energetic proton fluxes and associated microwave burst parameters. *J. Geophys. Res.* **87**, 3439–3448. doi:10.1029/JA087iA05p03439.

Kahler, S.W.: 1992, Solar flares and coronal mass ejections. *Annu. Rev. Astron. Astrophys.* **30**, 113–141. doi:10.1146/annurev.aa.30.090192.000553.

Kahler, S.W.: 2001, The correlation between solar energetic particle peak intensities and speeds of coronal mass ejections: effects of ambient particle intensities and energy spectra. *J. Geophys. Res.* **106**, 20947–20956. doi:10.1029/2000JA002231.

Kahler, S.W., Krucker, S., Szabo, A.: 2011, Solar energetic electron probes of magnetic cloud field line lengths. *J. Geophys. Res.* **116**, A01104. doi:10.1029/2010JA015328.

Kahler, S.W., Cliver, E.W., Cane, H.V., McGuire, R.E., Stone, R.G., Sheeley, N.R. Jr.: 1986, Solar filament eruptions and energetic particle events. *Astrophys. J.* **302**, 504–510. doi:10.1086/164009.

Klecker, B., Kunow, H., Cane, H.V., Dalla, S., Heber, B., Kecskemety, K., *et al.*: 2006, Energetic particle observations. *Space Sci. Rev.* **123**, 217–250. doi:10.1007/s11214-006-9018-9.

Klein, K.-L., Trottet, G., Klassen, A.: 2010, Energetic particle acceleration and propagation in strong CME-less flares. *Solar Phys.* **263**, 185–208. doi:10.1007/s11207-010-9540-5.

Klein, K.-L., Trottet, G., Samwel, S., Malandraki, O.: 2011, Particle acceleration and propagation in strong flares without major solar energetic particle events. *Solar Phys.* **269**, 309–333. doi:10.1007/s11207-011-9710-0.

Malandraki, O.E., Lario, D., Lanzerotti, L.J., Sarris, E.T., Geranios, A., Tsiropoula, G.: 2005, October/November 2003 interplanetary coronal mass ejections: ACE/EPAM solar energetic particle observations. *J. Geophys. Res.* **110**, A09S06. doi:10.1029/2004JA010926.

Marqué, C., Posner, A., Klein, K.-L.: 2006, Solar energetic particles and radio-silent fast coronal mass ejections. *Astrophys. J.* **642**, 1222–1235. doi:10.1086/501157.

Marubashi, K.: 1997, Interplanetary magnetic flux ropes and solar filaments. In: Crooker, N., Joselyn, J.A., Feynman, J. (eds.) *Coronal Mass Ejections*, *AGU Geophys. Monogr.* **99**, AGU, Washington, 147–156.

Masson, S., Aulanier, G., Pariat, E., Klein, K.-L.: 2012a, Interchange slip-running reconnection and sweeping SEP beams. *Solar Phys.* **276**, 199–217. doi:10.1007/s11207-011-9886-3.

Masson, S., Démoulin, P., Dasso, S., Klein, K.-L.: 2012b, The interplanetary magnetic structure that guides solar relativistic particles. *Astron. Astrophys.* **538**, A32. doi:10.1051/0004-6361/201118145.

Posner, A.: 2007, Up to 1-hour forecasting of radiation hazards from solar energetic ion events with relativistic electrons. *Space Weather* **5**, S05001. doi:10.1029/2006SW000268.

Ramaty, R., Mandzhavidze, N., Kozlovsky, B., Skibo, J.G.: 1993, Acceleration in solar flares: interacting particles versus interplanetary particles. *Adv. Space Res.* **13**, 275–284. doi:10.1016/0273-1177(93)90490-3.

Reames, D.V.: 1999, Particle acceleration at the Sun and in the heliosphere. *Space Sci. Rev.* **90**, 413–491. doi:10.1023/A:1005105831781.

Richardson, I.G., Cane, H.V.: 2010, Near-Earth interplanetary coronal mass ejections during solar cycle 23 (1996–2009): catalog and summary of properties. *Solar Phys.* **264**, 189–237. doi:10.1007/s11207-010-9568-6.

Richardson, I.G., Cane, H.V., von Rosenvinge, T.T.: 1991, Prompt arrival of solar energetic particles from far eastern events – the role of large-scale interplanetary magnetic field structure. *J. Geophys. Res.* **96**, 7853–7860. doi:10.1029/91JA00379.

Sammis, I., Tang, F., Zirin, H.: 2000, The dependence of large flare occurrence on the magnetic structure of sunspots. *Astrophys. J.* **540**, 583–587. doi:10.1086/309303.

Smith, E.J.: 2008, The global heliospheric magnetic field. In: Balogh, A., Lanzerotti, L.J., Suess, S.T. (eds.) *The Heliosphere Through the Solar Activity Cycle*, Praxis Publishing, Chichester, 79–150.

Torsti, J., Riihonen, E., Kocharov, L.: 2004, The 1998 May 2–3 magnetic cloud: an interplanetary "Highway" for solar energetic particles observed with SOHO/ERNE. *Astrophys. J.* **600**, 83–86. doi:10.1086/381575.

Tranquille, C., Sanderson, T.R., Marsden, R.G., Wenzel, K.-P., Smith, E.J.: 1987, Properties of a large-scale interplanetary loop structure as deduced from low-energy proton anisotropy and magnetic field measurements. *J. Geophys. Res.* **92**, 6 – 14. doi:10.1029/JA092iA01p00006.

Vandas, M., Odstrčil, D., Watari, S.: 2002, Three-dimensional MHD simulation of a loop-like magnetic cloud in the solar wind. *J. Geophys. Res.* **107**(A9), SSH2-1. doi:10.1029/2001JA005068.

Vršnak, B., Sudar, D., Ruždjak, D.: 2005, The CME-flare relationship: are there really two types of CMEs? *Astron. Astrophys.* **435**, 1149 – 1157. doi:10.1051/0004-6361:20042166.

Vršnak, B., Sudar, D., Ruždjak, D., Žic, T.: 2007, Projection effects in coronal mass ejections. *Astron. Astrophys.* **469**, 339 – 346. doi:10.1051/0004-6361:20077175.

Wall, J.V., Jenkins, C.R.: 2003, *Practical Statistics for Astronomers*, Cambridge University Press, Cambridge.

Wang, Y., Zhang, J.: 2008, A statistical study of solar active regions that produce extremely fast coronal mass ejections. *Astrophys. J.* **680**, 1516 – 1522. doi:10.1086/587619.

Yashiro, S., Gopalswamy, N.: 2009, Statistical relationship between solar flares and coronal mass ejections. In: Gopalswamy, N., Webb, D.F. (eds.) *IAU Symp.* **257**, 233 – 243. doi:10.1017/S1743921309029342.

Yashiro, S., Gopalswamy, N., Michalek, G., St. Cyr, O.C., Plunkett, S.P., Rich, N.B., Howard, R.A.: 2004, A catalog of white light coronal mass ejections observed by the SOHO spacecraft. *J. Geophys. Res.* **109**, A07105. doi:10.1029/2003JA010282.

Yeh, C.-T., Ding, M.D., Chen, P.F.: 2005, Kinetic properties of CMEs corrected for the projection effect. *Solar Phys.* **229**, 313 – 322. doi:10.1007/s11207-005-6883-4.

Zhang, J., Dere, K.P., Howard, R.A., Kundu, M.R., White, S.M.: 2001, On the temporal relationship between coronal mass ejections and flares. *Astrophys. J.* **559**, 452 – 462. doi:10.1086/322405.